

We are IntechOpen, the world's leading publisher of Open Access books Built by scientists, for scientists

6,900

Open access books available

185,000

International authors and editors

200M

Downloads

Our authors are among the

154

Countries delivered to

TOP 1%

most cited scientists

12.2%

Contributors from top 500 universities



WEB OF SCIENCE™

Selection of our books indexed in the Book Citation Index
in Web of Science™ Core Collection (BKCI)

Interested in publishing with us?
Contact book.department@intechopen.com

Numbers displayed above are based on latest data collected.
For more information visit www.intechopen.com



Numerical Investigation of Hybrid-Stabilized Argon-Water Electric Arc Used for Biomass Gasification

J. Jeništa¹, H. Takana², H. Nishiyama², M. Bartlová³, V. Aubrecht³, P. Křenek¹, M. Hrabovský¹, T. Kavka¹, V. Sember¹ and A. Mašláni¹

¹*Institute of Plasma Physics, AS CR, v.v.i., Thermal Plasma Department, Praha*

²*Institute of Fluid Science, Tohoku University, Sendai, Miyagi,*

³*Brno University of Technology, Brno*

^{1,3}*Czech Republic*

²*Japan*

1. Introduction

Plasma generators with arc discharge stabilization by water vortex exhibit special performance characteristics; such as high outlet plasma velocities (up to $7\,000\text{ m}\cdot\text{s}^{-1}$), temperatures ($\sim 30\,000\text{ K}$), plasma enthalpy and, namely, high powder throughput, compared to commonly used gas-stabilized (Ar, He) torches (Hrabovský et al., 1997). In a water-stabilized arc, the stabilizing wall is formed by the inner surface of water vortex which is created by tangential water injection under high pressure ($\sim 10\text{ atm.}$) into the arc chamber. Evaporation of water is induced by the absorption of a fraction of Joule power dissipated within the conducting arc core. Further heating and ionization of the steam are the principal processes which produce water plasma. The continuous inflow and heating lead to an overpressure and plasma is accelerated towards the nozzle exit. The arc properties are thus controlled by the radial energy transport from the arc core to the walls and by the processes influencing evaporation of the liquid wall.

A combination of gas and vortex stabilization has been utilized in the so-called hybrid-stabilized electric arc, its principle is shown in Fig.1. In the hybrid H_2O -Ar plasma arc the discharge chamber is divided into the short cathode part where the arc is stabilized by tangential argon flow in the axial direction, and the longer part which is water-vortex-stabilized. This arrangement not only provides additional stabilization of the cathode region and protection of the cathode tip, but also offers the possibility of controlling plasma jet characteristics in wider range than that of pure gas or liquid-stabilized torches (Březina et al., 2001; Hrabovský et al., 2003). The arc is attached to the external water-cooled rotating disc anode a few mm downstream of the torch orifice. The characteristics of the hybrid-stabilized electric arc were measured and the effect of gas properties and flow rate on plasma properties and gas-dynamic flow characteristics of the plasma jet were studied. Experiments (Březina et al., 2001; Hrabovský et al., 2006) proved that plasma mass flow rate,

velocity and momentum flux in the jet can be controlled by changing mass flow rate in the gas-stabilized section, whereas thermal characteristics are determined by processes in the water-stabilized section. The domain for numerical calculation is shown in Fig. 1 by a dashed line and includes the discharge area between the outlet nozzle for argon and the near-outlet region of the hybrid plasma torch.

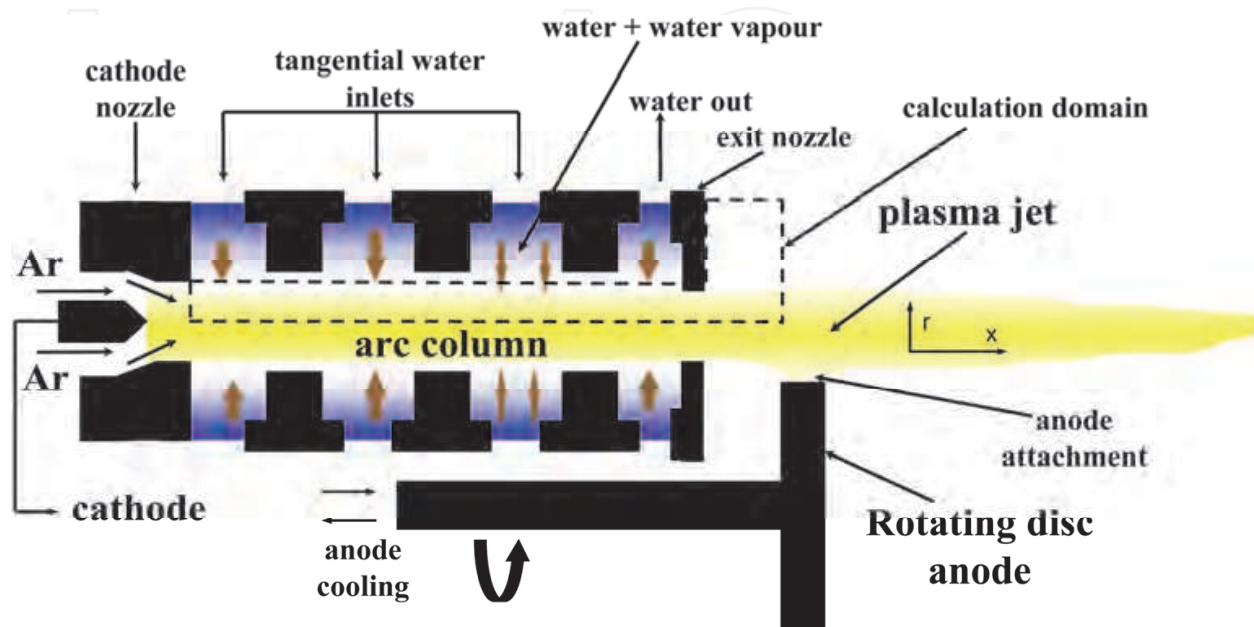


Fig. 1. Principle of hybrid plasma torch WSP®H with combined gas (Ar) and vortex (water) stabilizations. Water is injected tangentially and creates vortex in the chamber. The arc burns between the cathode, made of a small piece of zirconium pressed into a copper rod, and the water-cooled anode rotating disc. The calculation domain is shown by a dashed line.

The hybrid arc has been used at IPP AS CR, v.v.i., in the plasma spraying torch WSP®H (160 kW) for spraying metallic or ceramic powders injected into the plasma jet (Fig. 2). Recently, an experimental plasmachemical reactor PLASGAS (Fig. 3) equipped with the spraying torch WSP®H has been started for the innovative and environmentally friendly plasma treatment of waste streams with a view to their sustainable energetic and chemical valorization and to a reduction of the emission of greenhouse gases (Van Oost et al., 2006, 2008). Pyrolysis of biomass was experimentally studied in the reactor using crushed wood and sunflower seeds as model substances. Syngas with a high content of hydrogen and CO was produced.

This work aims to study properties and processes in the hybrid arc for high currents (300-600 A) and argon mass flow rates (22.5-40 standard liters per minute, slm). In contrast to our previous investigation (Jeništa, 2004; Jeništa et al., 2007), a special attention is devoted to the flow structure and temperature field in the discharge when the local Mach number is higher than one. Our former results indicated the possibility (Jeništa, 2004) and also proved the existence (Jeništa et al., 2008) of supersonic flow regime for currents higher or equal to 500 A. In addition, a detailed comparison of the calculated results with experiments is presented in this study.

Section 2 gives information about the model assumptions, plasma properties, boundary conditions and the numerical scheme. Section 3 reveals the most important findings such as thermal and fluid dynamic characteristics of plasma within the discharge and in the near-outlet regions, along with power losses from the arc and comparison of calculated results (temperature and velocity profiles near the nozzle exit) with experiments.

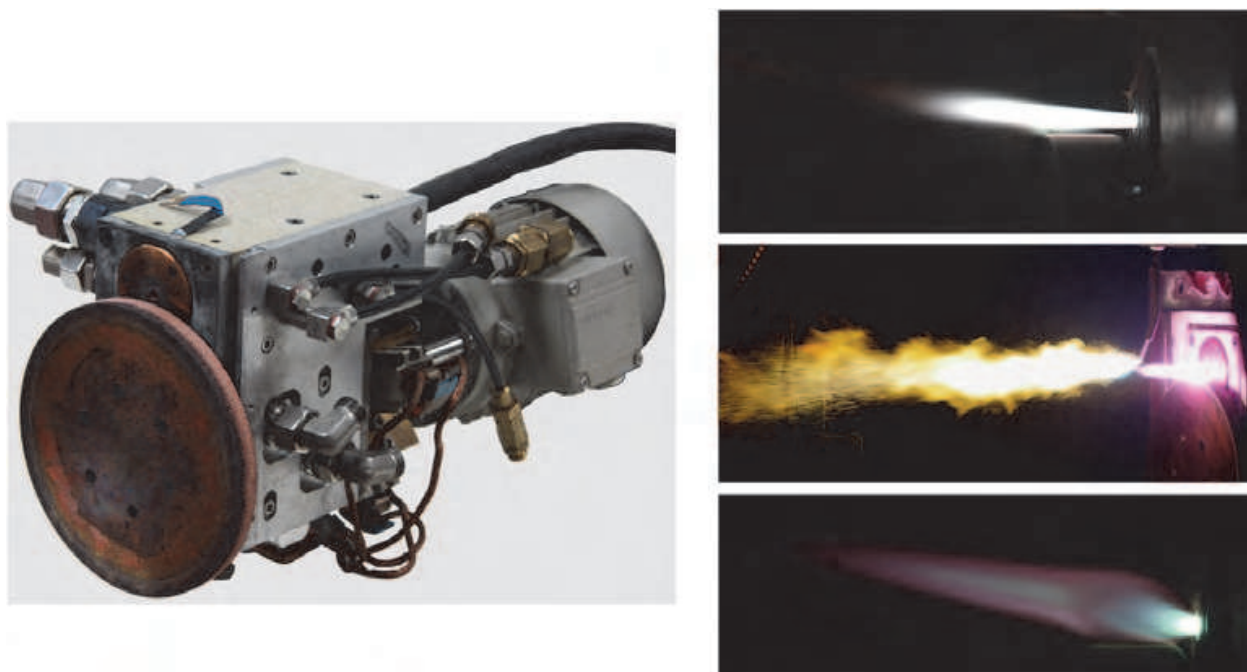


Fig. 2. The plasma spraying torch WSP®H with hybrid stabilization (left), i.e. the combined stabilization of arc by axial gas flow (Ar or N₂) and water vortex. The external rotating disk anode is made of copper. Images of plasma jets produced by WSP®H (right) from the mixture of steam and argon for different operational conditions: 300 A and 24 slm of argon (top), spraying of Cu particles at 500 A and 36 slm of argon (middle), supersonic jet at 300 A, 12 slm of argon at 10 kPa of surrounding atmosphere (bottom).

2. Physical model and numerical implementation

2.1 Assumptions and the set of equations

The following assumptions for the model are applied:

1. the numerical model is two-dimensional with the discharge axis as the axis of symmetry,
2. plasma flow is laminar/turbulent and compressible in the state of local thermodynamic equilibrium,
3. argon and water create a uniform mixture in the arc chamber,
4. only self-generated magnetic field by the arc itself is considered,
5. gravity effects are negligible,
6. the partial characteristics and the net emission coefficients methods (models) for radiation losses from the arc are employed,
7. all the transport, thermodynamic and radiation properties are dependent on temperature, pressure and argon molar content.

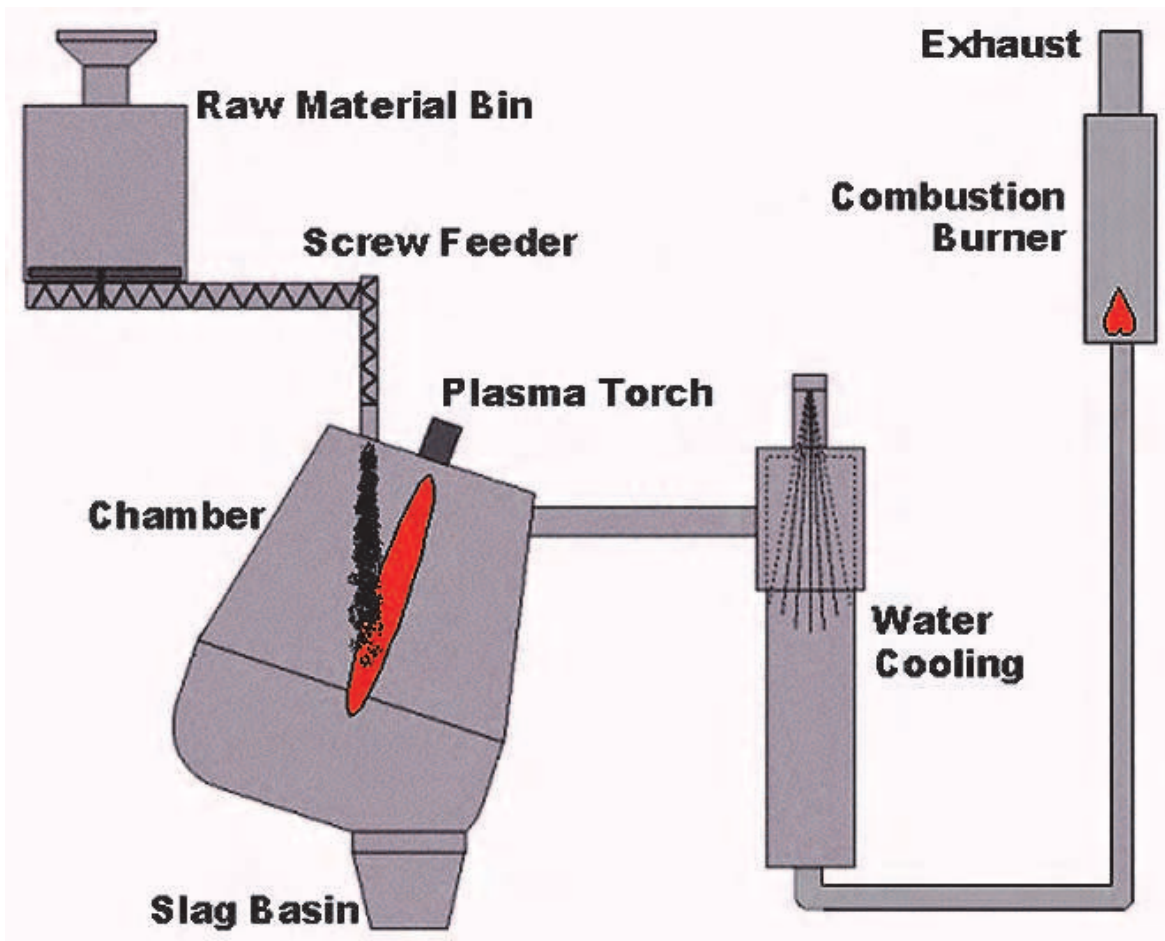


Fig. 3. Schematic diagram of the experimental reactor for plasma pyrolysis and gasification.

A few comments should be mentioned on these assumptions:

1. The cylindrical discharge chamber (Fig. 1) is divided into several sections by the baffles with central holes. Water is injected tangentially into the chamber by three sets of three inlet holes (totally 9 holes) placed equidistantly along the circumference at angles of 120° . The inner diameter of the water vortex is determined by the diameter of the holes in the baffles. Water is usually pumped under pressures of 0.39 MPa (0.6 MPa) with flow rates of 10 l min^{-1} (16 l min^{-1}). Higher pressures insure better hydrodynamic stability of the arc. Since water flows in a closed circuit, it is also exhausted at two positions along the arc chamber.

In order to see the flow structure near the outlet, we included in our calculation domain also the near-outlet region which extends up to 20 mm from the nozzle exit. In experiment, the distance from the nozzle exit to the anode can be changed from 5 to 20 mm. It can be expected that regions close to the nozzle exit will remain undisturbed by the presence of the anode, while the more distant regions (15-20 mm) will be influenced by 3D effects (the anode jet and anode processes), provided the anode is placed somewhere 20 mm from the nozzle exit.

It comes out from these considerations that the two-dimensional assumption is valid in major part of the domain due to a) cylindrical symmetry of the discharge chamber setup, b) tangential injection of water through the holes along the circumference, and c) the flexible distance between the nozzle exit and anode.

2. The assumption of laminar flow is based on experiments, showing the laminar structure of the plasma flowing out of the discharge chamber in the space between the nozzle exit and the anode. The laminar flow has been observed for currents up to 600 A. It comes out from our previous calculation that Reynolds number based on the outlet diameter 6 mm reaches in the axial region 13 000 at maximum and decreases to 300 in arc fringes. The type of flow inside the discharge chamber is questionable since no diagnostics is able to see inside the chamber and it is not clear if the laminar plasma stream is a result of laminarization of the plasma flow at the outlet. To check possible deviations from the laminar model, we have employed Large Eddy Simulation (LES) with the Smagorinsky sub-grid scale model. It was proved that simulations for laminar and turbulent regimes give nearly the same results, so that the plasma flow can be considered more or less laminar for the operating conditions and simplified discharge geometry in the present study. The maximum detected discrepancy between the turbulent and laminar models is 7 % for the relative temperature difference at the arc axis 2 mm downstream of the nozzle exit for 500 A and 40 slm of argon. For reasons of generality, all the results presented here were calculated using the LES turbulent model.
3. The assumption of a complete (uniform) mixing is a simplification of a reality since, based on experiments, argon and water species do not mix homogeneously in the hybrid torch, especially at lower currents. This assumption was discussed in more detail in (Jeništa, 2004) and it was concluded that this assumption can underestimate temperature and velocity in the axial discharge region to some extent.

The complete set of conservation equations representing the mass, electric charge, momentum and energy transport of such plasma can be written in the vector notation as follows:

continuity equation:

$$\frac{\partial \rho}{\partial t} + \frac{1}{r} \frac{\partial}{\partial r}(\rho v r) + \frac{\partial}{\partial z}(\rho u) = 0 \quad (1)$$

momentum equations:

$$\begin{aligned} \frac{\partial}{\partial t}(\rho u) + \frac{\partial}{\partial r}(\rho u v) + \frac{\partial}{\partial z}(\rho u u) = & -\frac{\partial p}{\partial z} + j_r B_\theta - \frac{2}{3} \frac{\partial}{\partial z} \left[\mu \left(\frac{1}{r} \frac{\partial}{\partial r}(r v) + \frac{\partial u}{\partial z} \right) \right] + \\ & \frac{\partial}{\partial z} \left(2\mu \frac{\partial u}{\partial z} \right) + \frac{1}{r} \frac{\partial}{\partial r} \left[r \mu \left(\frac{\partial u}{\partial r} + \frac{\partial v}{\partial z} \right) \right] \end{aligned} \quad (2)$$

$$\begin{aligned} \frac{\partial}{\partial t}(\rho v) + \frac{\partial}{\partial r}(\rho v v) + \frac{\partial}{\partial z}(\rho u v) = & -\frac{\partial p}{\partial r} - j_x B_\theta - \frac{2}{3} \frac{\partial}{\partial r} \left[\mu \left(\frac{1}{r} \frac{\partial}{\partial r}(r v) + \frac{\partial u}{\partial z} \right) \right] + \frac{\rho v^2}{r} + \\ & \frac{1}{r} \frac{\partial}{\partial r} \left(2\mu r \frac{\partial v}{\partial r} \right) - \frac{2\mu v}{r^2} + \frac{\partial}{\partial z} \left[\mu \left(\frac{\partial u}{\partial r} + \frac{\partial v}{\partial z} \right) \right] \end{aligned} \quad (3)$$

energy equation:

$$\begin{aligned} \frac{\partial e}{\partial t} + \frac{1}{r} \frac{\partial}{\partial r} \left[r \left\{ (e + p) v - \lambda \frac{\partial T}{\partial r} \right\} \right] + \frac{\partial}{\partial z} \left[(e + p) u - \lambda \frac{\partial T}{\partial z} \right] = \\ \frac{1}{r} \frac{\partial}{\partial r} \left[r (\tau_{rr} v + \tau_{rz} u) \right] + \frac{\partial}{\partial z} (\tau_{rz} v + \tau_{zz} u) + j_r E_r + j_z E_z - R \end{aligned} \quad (4)$$

charge continuity equation:

$$\frac{1}{r} \frac{\partial}{\partial r} \left(r \sigma \frac{\partial \Phi}{\partial r} \right) + \frac{\partial}{\partial z} \left(\sigma \frac{\partial \Phi}{\partial z} \right) = 0 \quad (5)$$

equation of state:

$$p = \rho R_g T . \quad (6)$$

Here z and r are the axial and radial coordinates, u , v and w are the axial, radial and tangential components of the velocity respectively, ρ is the mass density, μ is the viscosity (in the case of LES model, the turbulent contribution μ_{turb} is also added) p is the pressure, B_θ is the magnetic field strength, e is the density of energy produced or dissipated in the unit volume (internal and kinetic), T is the temperature, τ is the viscous stress tensor, j_z and j_r are the axial and radial components of the current density, E_z and E_r are the axial and radial components of the electric field strength, Φ is the electric potential, R is the source term for the radiation losses and R_g is the molar gas constant. The magnetic field strength B_θ is calculated from the Biot-Savart law, the current density \vec{j} from the Ohm's law $\vec{j} = \sigma \cdot \vec{E}$.

2.2 Properties of argon-water plasma mixture

The water-argon mixture can be described by the formula $(H_2O)_{(1-q)} Ar_q$ where the argon molar amounts q were chosen from 0 to 1 with the step of 0.1. The total number of 35 chemical species was considered (Křenek, 2008). For the temperature range 400 - 20 000 K we supposed the following decomposition products: e (electrons), H , O , Ar , O^+ , O^{2+} , O^{3+} , O^- , O_2 , O_2^+ , O_2^- , O_3 , H^+ , H^- , H_2 , H_2^+ , H_3^+ , OH , OH^+ , OH^- , HO_2 , HO_2^- , H_2O , H_2O^+ , H_3O^+ , H_2O_2 , Ar^+ , Ar^{2+} , Ar^{3+} . For the temperature range 20 - 50 000 K the set of products is somewhat different, including also multiply charged ions: e (electrons), H , O , Ar , O^+ , O^{2+} , O^{3+} , O^{4+} , O^{5+} , O^{6+} , H^+ , Ar^+ , Ar^{2+} , Ar^{3+} , Ar^{4+} , Ar^{5+} , Ar^{6+} . The calculations were performed using the modified Newton method for the solution of nonlinear equations system which is composed of equations of Saha and mass action law type expressing individual complex components by the help of basic ones (e, H, O, Ar). The system is completed by the usual particle and charge balance assuming quasineutrality and equilibrium.

The thermodynamic properties and the transport coefficients of this gas mixture were calculated according to the Chapman-Enskog method in the 4th approximation described e.g. in (Křenek & Něnička, 1984) for temperatures 400-50 000 K (Křenek, 2008) and pressures 0.1-0.3 MPa in the local thermodynamic equilibrium.

Two radiation models are implemented in the energy equation for energy losses from the argon-water plasma: 1) the net emission coefficients for the required arc radius of 3.3 mm, and 2) the partial characteristics method, both of them for different molar fractions of argon and water plasma species in dependence on temperature and pressure. Continuous radiation due to photorecombination and "bremsstrahlung" processes has been included in the calculation as well as discrete radiation consisting of thousands of spectral lines. Broadening mechanisms of atomic and ionic spectral lines due to Doppler, resonance and Stark effects have been considered. The numbers of oxygen and argon lines included in the

calculation are O (93 lines), O^+ (296), O_2^+ (190), Ar (739), Ar^+ (2781), Ar^{2+} (403), Ar^{3+} (73). In addition, molecular bands of O_2 (Schuman-Runge system), H_2 (Lyman and Verner systems), OH (transition $A^2\Sigma^+ \rightarrow X^2\Pi_i$) and H_2O (several transitions) have been also implemented (Bartlová & Aubrecht, 2006). Absorption coefficient as a function of wavelength has been calculated from infrared to far ultraviolet regions and the tables of partial characteristics for 1 000 – 35 000 K. The net emission coefficients model used here is a special case of the partial characteristics model with zero partial sink, $\Delta Sim = 0$.

2.3 Boundary conditions and numerical scheme

The calculation region and the corresponding boundary conditions are presented in Fig. 4. The dimensions are 3.3 mm for the radius of the discharge region, 20 mm for the radius of the outlet region and 78.32 mm for the total length. These dimensions agree with the hybrid torch experimental setup.

- a. *Inlet boundary (AB)* is represented by the nozzle exit for argon. Along this boundary we assume the zero radial velocity component, $v = 0$. Because of the lack of experimental data, the temperature profile $T(r, z = 0)$ and the electric field strength $E_z = -\partial\Phi/\partial z = const.$ for a given current are calculated at this boundary, before the start of the fluid-dynamic calculation itself, iteratively from the Elenbaas-Heller equation including the radiation losses from the arc (our previous numerical experiments proved a weak dependence of the form of the boundary temperature profile on the overall solution). The inlet velocity profile $u(r)$ for argon plasma for the obtained temperature profile $T(r, z = 0)$ is pre-calculated from the axial momentum equation under the assumption of fully developed flow.
- b. *Axis of symmetry (BC)*. The zero radial velocity and symmetry conditions for the temperature, axial velocity and electric potential are specified here, i.e. $\partial T/\partial r = \partial u/\partial r = \partial\Phi/\partial r = 0, v = 0$.
- c. *Arc gas outlet plane (CD)*. The zero electric potential $\Phi = 0$ (the reference value) and zero axial derivatives of the temperature and radial velocity are defined at CD, $\partial T/\partial z = \partial v/\partial z = 0$. Values of the axial velocity are interpolated from the inner grid points.
- d. *Arc gas outlet plane (DE)*. The zero radial velocity and zero radial derivatives of the temperature, axial velocity and electric potential are defined here, $\partial T/\partial r = \partial u/\partial r = \partial\Phi/\partial r = 0, v = 0$. Pressure is fixed at 1 atmosphere, $p = 1 \text{ atm}$.
- e. *Outlet wall and the nozzle (EF)*. We specify no slip conditions for velocities, $u = v = 0$, constant values of E_r and E_z ($\partial\Phi/\partial z = \partial\Phi/\partial r = 0$) and $T(r, z) = 773 \text{ K}$ (500° C) for the temperature of the nozzle.
- f. *Water vapor boundary (FA)*. Along this line we specify the so-called “effective water vapor boundary”, named in Fig. 4 as the “water vapor boundary” with a prescribed temperature of water vapor $T(R = 3.3 \text{ mm}, z) = 773 \text{ K}$. This is a numerical simplification of a more complex physical reality assumed near the phase transition water-vapor in the discharge chamber. The shape of the phase transition between water and vapor in the discharge chamber is not experimentally known and it is unclear so far if the structure of the transition is simple or very complicated, for example, with a time-dependent form. Various irregularities in the transition such as

splitting of the phase transition or water drops in the vapor phase can increase complexity of the transition. In (Jeništa, 2003a) the iteration procedure for determination of the mass flow rate and the radius of the “water vapor boundary” for each current was proposed, based on comparison with available experimental temperature and velocity at the outlet and the electric potential drop in the chamber. It was concluded that the best fit between experiment and numerical simulation for all currents exists for a mean arc radius of 3.3 mm. The corresponding values of water mass flow rates are 0.228 g s^{-1} (300 A), 0.286 g s^{-1} (350 A), 0.315 g s^{-1} (400 A), 0.329 g s^{-1} (500 A), 0.363 g s^{-1} (600 A). The magnitude of the radial inflow velocity is calculated from the definition of mass flow rate

$$v(R) = \frac{\dot{m}}{2\pi R \sum_{\Delta z} \rho(R, z) \Delta z},$$

where $\rho(R, z)$ is a function of pressure and thus dependent on the axial position z , Δz is the distance between the neighboring grid points.

Because of practically zero current density in cold vapor region (no current goes outside of the lateral domain edges), the radial component of the electric field strength is put zero, i.e., $E_r = 0$. The axial velocity component is set to zero, $u = 0$. Since we do not solve here the equation for tangential velocity component w , distribution of w in the discharge for the presented results was taken from our previous calculations (Jeništa et al., 1999a) solved by the SIMPLER iteration procedure (Patankar, 1980) which enables calculation of w for axisymmetric case, i.e., w as a function of z and r coordinates. The w velocity acts here only through the centrifugal force $\rho w^2/r$ in the radial momentum equation (3).

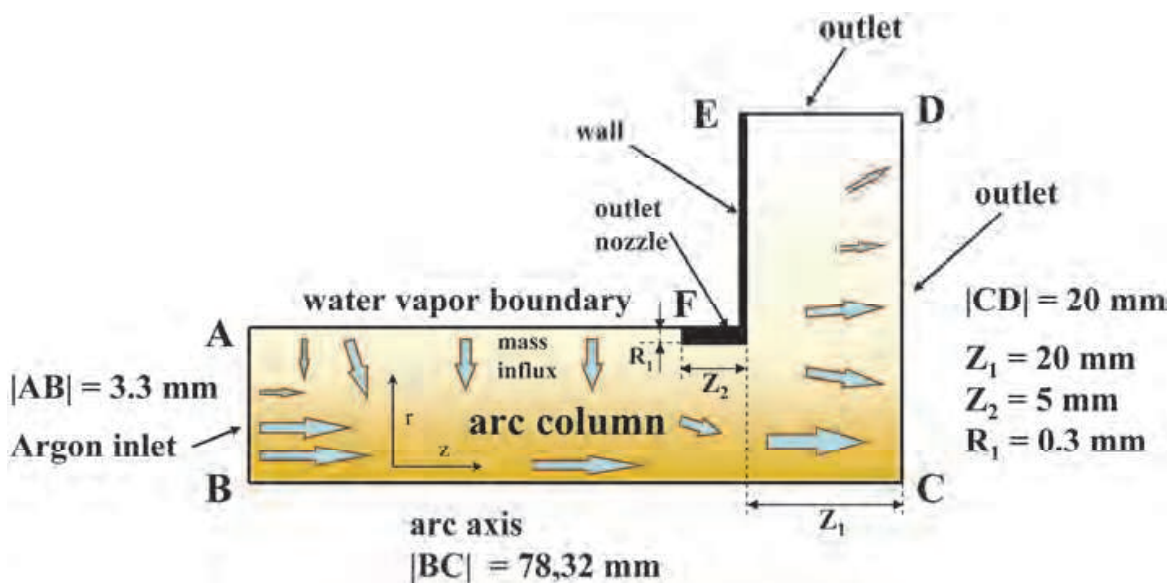


Fig. 4. Discharge area geometry. Inlet boundary (AB) is represented by the nozzle exit for argon. The length of the discharge region is 58.32 mm, the length of the outlet is 20 mm. Along the line FE we specify the outlet nozzle and the wall of the hybrid plasma torch equipment.

For time integration of (1)-(4), LU-SGS (Lower-Upper Symmetric Gauss-Seidel) algorithm (Jameson & Yoon, 1987; Yoon & Jameson, 1988), coupled with Newtonian iteration method are used for the integration of discretized equations in time and space. To resolve compressible phenomena accurately, the Roe flux differential method (Roe, 1981) coupled with the third-order MUSCL-type (Monotone Upstream-centered Schemes for Conservation Laws) TVD (Total Variation Diminishing) scheme (van Leer, 1979) are used for convective term. The electric potential from (5) is solved in a separate subroutine by the TDMA (Tri-Diagonal Matrix Algorithm) line-by-line method. From (1-4) we obtain ρ , $\rho\bar{u}$, e and Φ . Pressure is determined from the pressure dependence of the internal energy $U(p, T) = e(p, T) - 0.5\rho|\bar{u}|^2$ and temperature is calculated from the equation of state (6) $p/\rho = R_g(p, T) \cdot T$, using the pre-calculated values of the product $R_g(p, T) \cdot T$ as a function of temperature, pressure and argon molar fraction in the mixture (Křenek, 2008).

The computer program is written in the FORTRAN language. The task has been solved on an oblique structured grid with nonequidistant spacing. The total number of grid points was 38 553, with 543 and 71 points in the axial and radial directions respectively.

3. Results of calculation

3.1 Thermal, fluid flow and electrical characteristics of the plasma

Calculations have been carried out for the currents 300, 400, 500 and 600 A. Mass flow rate for water-stabilized section of the discharge was taken for each current between 300 and 600 A from our previously published work (Jeništa, 2003a; Jeništa, 2003b), where it was determined iteratively as a minimum difference between numerical and experimental outlet quantities. The resulting values are $0.228 \text{ g} \cdot \text{s}^{-1}$ (300 A), $0.315 \text{ g} \cdot \text{s}^{-1}$ (400 A), $0.329 \text{ g} \cdot \text{s}^{-1}$ (500 A), $0.363 \text{ g} \cdot \text{s}^{-1}$ (600 A). Argon mass flow rate was varied in agreement with experiments in the interval from 22.5 slm to 40 slm, namely 22.5, 27.5, 32.5 and 40 slm. It was proved in experiments (Kavka et al., 2007) that part of argon is taken away before it reaches the torch exit because argon is mixed with vapor steam and removed to the water system of the torch. The amount of argon transferred in such a way from the discharge is at least 50 % for currents studied. Since the present model does not treat argon and water as separate gases and the mechanism of argon removal is not included in the model, we consider in the calculations that argon mass flow rate present in the discharge equals one-half of argon mass flow rate at the torch inlet. A relatively high values of argon mass flow rate, used also in experiment, were chosen here to demonstrate compressible phenomena.

Fig. 5 shows velocity, temperature, pressure and the Mach number in the outlet nozzle and near-outlet regions for 600 A, water mass flow rate of $0.363 \text{ g} \cdot \text{s}^{-1}$ and 40 slm of argon. The partial characteristics method for radiation losses is employed. The results shown here demonstrate the largest magnitude fluctuations of velocity, temperature, pressure and the Mach number just after the jet exhausts from the torch nozzle among all the studied currents and argon mass flow rates. Supersonic flow structure in the near-outlet region is obvious with clearly distinguished shock diamonds with the maximum Mach number about 1.6 with $10\,500 \text{ m} \cdot \text{s}^{-1}$. The corresponding velocity and the Mach number maxima overlap with the temperature and pressure minima and vice versa. Since the pressure decreases at the torch exit to a nearly atmospheric pressure, the computed contours correspond to an under-expanded atmospheric-pressure plasma jet.

The corresponding axial profiles of the Mach number, pressure, temperature and velocity along the arc axis downstream from the nozzle orifice (the axial position 58.32 mm) for the same run are presented in Fig. 6. Several successive wave crests and troughs along the axis for each of the physical parameters is a typical feature of supersonic fluid flow. The fluctuation of presented quantities is between 1.1-1.7 for the Mach number, 0.7-1.4 atm. for the pressure, 7 200-10 000 m · s⁻¹ for the velocity and 18 000-23 500 K for the temperature.

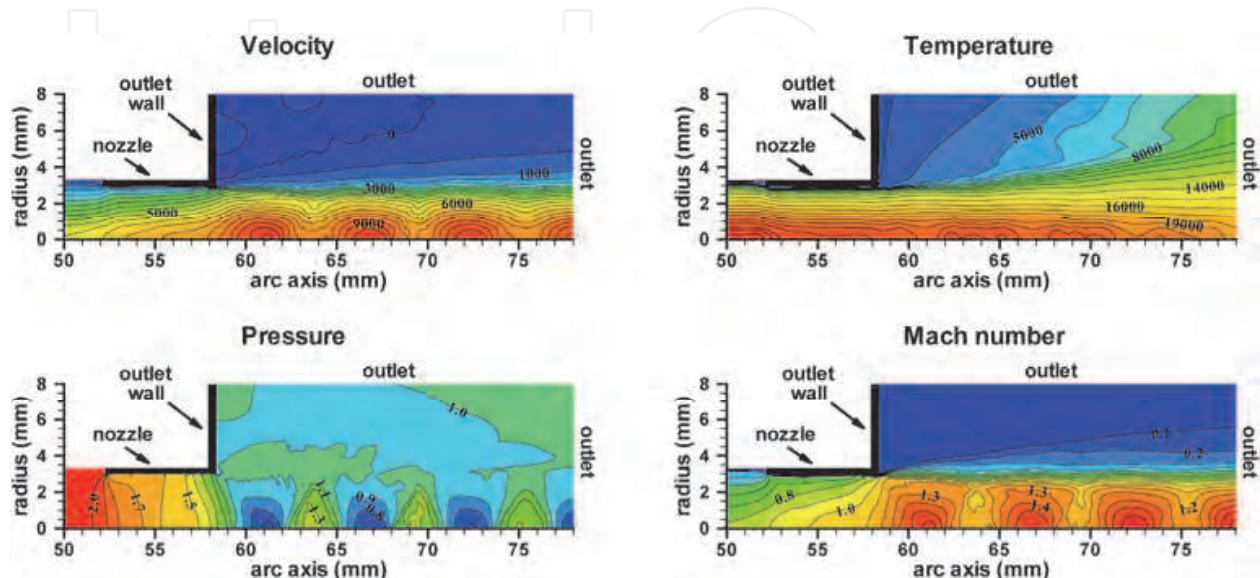


Fig. 5. Velocity, temperature, pressure and the Mach number contours in the outlet nozzle and near-discharge regions for the 600 A arc discharge. Water mass flow rate is 0.363 g s⁻¹, argon mass flow rate is 40 slm (standard liters per minute). Partial characteristics radiation model is employed. Supersonic flow structure is obvious with clearly distinguished shock diamonds. The maximum Mach number reaches 1.6. Contour increments are 500 m s⁻¹ for velocity, 1 000 K for temperature, 0.1 atm for pressure and 0.1 for the Mach number.

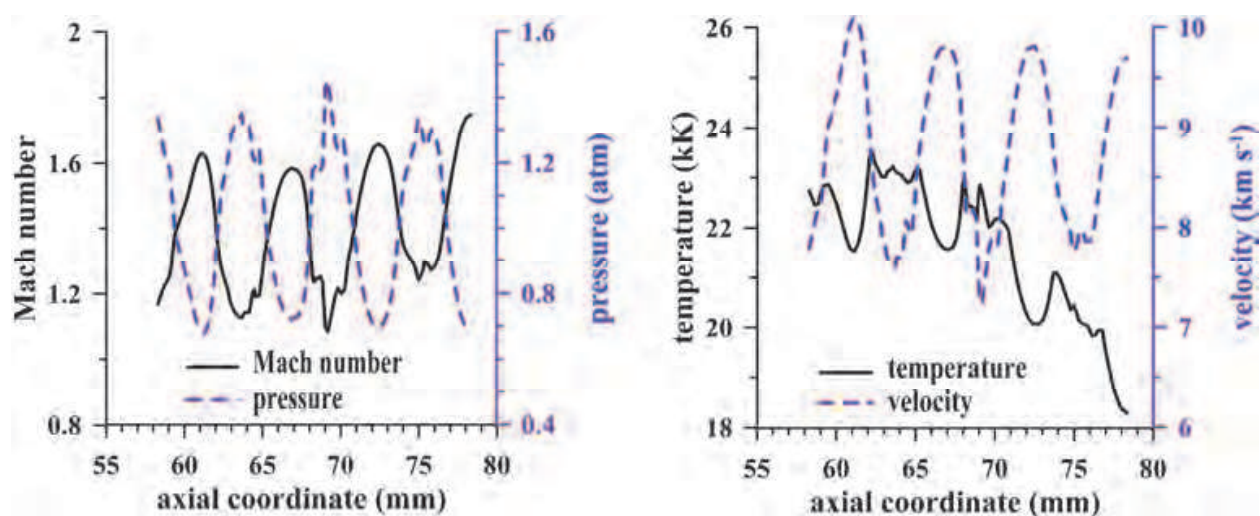


Fig. 6. Profiles of the Mach number, pressure, temperature and velocity along the arc axis from the nozzle orifice. Supersonic outlet with distinguished shock diamonds. 600 A, argon mass flow rate 40 slm, partial characteristics radiation model.

Fig. 7 displays temperature and velocity fields in the discharge and the near-outlet regions for a) 500 and b) 600 A with water mass flow rates of $0.329 \text{ g} \cdot \text{s}^{-1}$ (500 A), $0.363 \text{ g} \cdot \text{s}^{-1}$ (600 A) (Jeništa, 2003a) and argon mass flow rate of $0.554 \text{ g} \cdot \text{s}^{-1}$ (one half of 40 slm). The net emission coefficients radiation model is employed. Orientation of the calculation domain is the same as in Figs. 1, 4. Since the ratio of the axial to the radial dimensions of the calculation domain is ~ 24 the scaling of the radial and axial coordinates is not proportional to make the contours inside the discharge region clearly visible. Argon flows axially into the domain, whereas water evaporates in the radial direction from the “water vapor boundary”. Both the results for 500 and 600 A exhibit supersonic under-expanded plasma flow regime but a progression from weak to highly-pronounced shock diamonds structure at 600 A is obvious. The maximum velocities are $7\,200 \text{ m} \cdot \text{s}^{-1}$ (500 A) and $9\,400 \text{ m} \cdot \text{s}^{-1}$ (600 A) near the axial position of 60 mm. Further downstream the velocity amplitudes decrease due to viscosity dissipation and due to the reduction of the difference between the jet static pressure and back pressure.

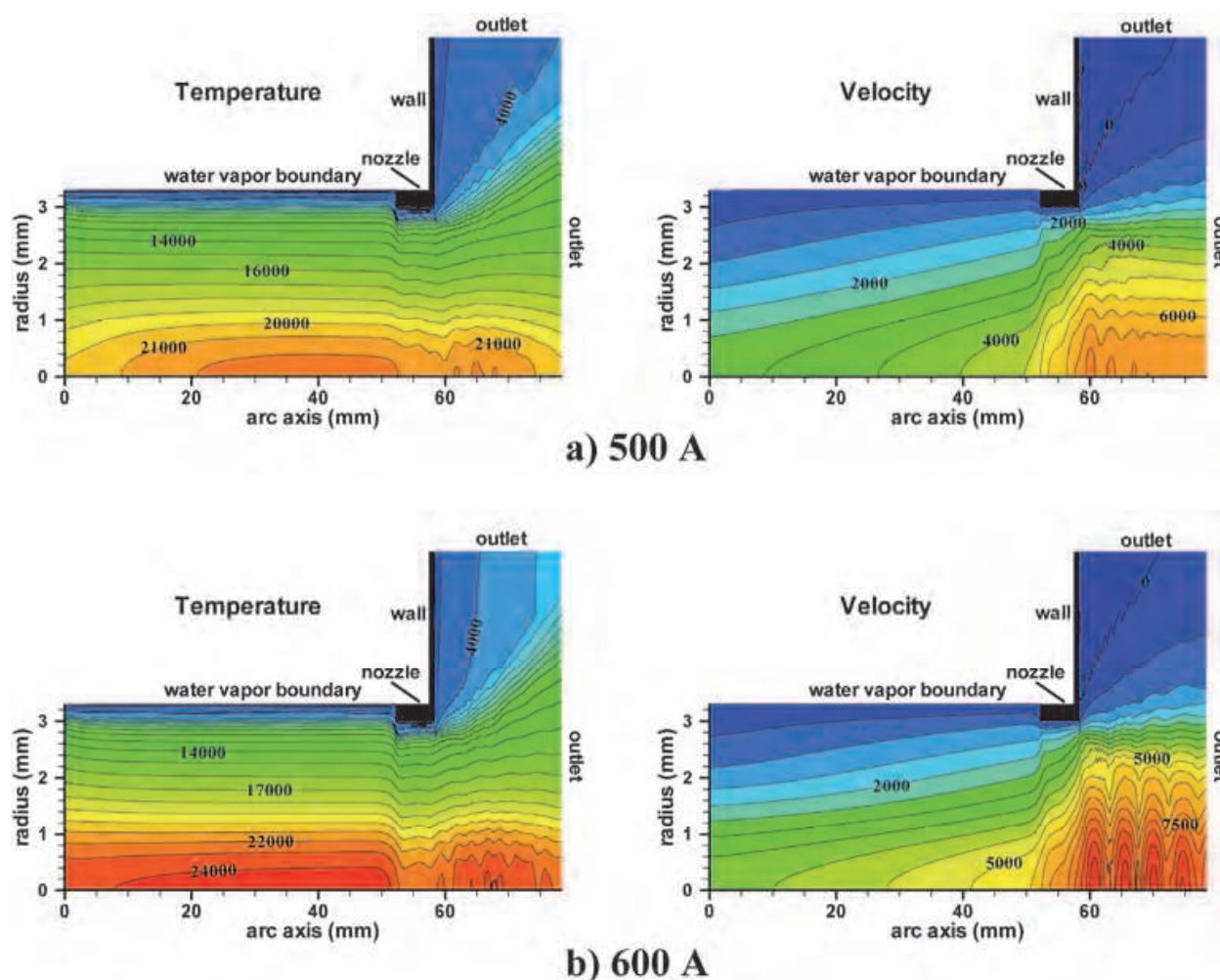


Fig. 7. Temperature and velocity contours for a) 500 A and b) 600 A arcs, net emission coefficients model. Water mass flow rates are $0.329 \text{ g} \cdot \text{s}^{-1}$ (500 A) and $0.363 \text{ g} \cdot \text{s}^{-1}$ (600 A); argon mass flow rate is 40 slm for both currents. Progression of a supersonic flow structure at the outlet is clearly visible. Contour increments are $1\,000 \text{ K}$ for temperature and $500 \text{ m} \cdot \text{s}^{-1}$ for velocity.

The impact of reabsorption of radiation on the distribution of temperature and velocity within the discharge and the near-outlet regions for 600 A is obvious in Fig. 8. The partial characteristics model gives lower temperatures and higher velocities at the outlet region. Similar results have been proved for all currents and argon mass flow rates.

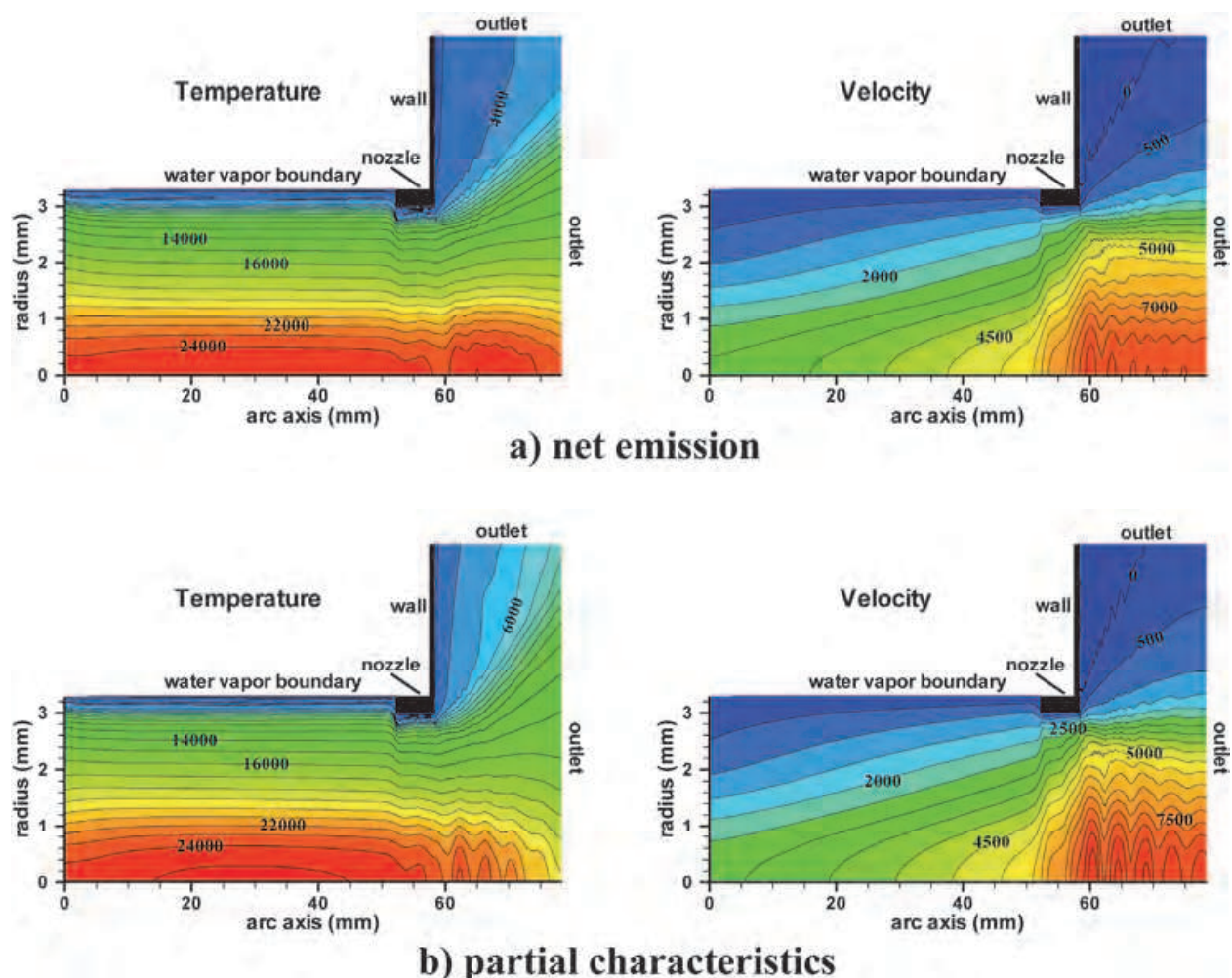


Fig. 8. Temperature and velocity contours for the net emission a) and partial characteristics b) models, 600 A, 27 slm of argon, water mass flow rate $0.363 \text{ g} \cdot \text{s}^{-1}$. The partial characteristics model gives lower temperatures and higher velocities at the outlet region. Contour increments are 1 000 K for temperature and $500 \text{ m} \cdot \text{s}^{-1}$ for velocity.

Fig. 9 presents the radial profiles of the Mach number 2 mm downstream of the nozzle exit with the argon mass flow rate of 40 slm. It is clearly demonstrated that for currents higher than 400 A, a supersonic rare plasma in the central parts of the discharge is surrounded by a subsonic, much denser but still hot plasma. Due to generally higher velocities and lower temperatures near the outlet the partial characteristics model gives higher values of the Mach number; the difference regarding the net emission coefficients model is below 0.1 at the arc axis.

Different flow structures for currents between 300 and 600 A and 32 slm of argon are visible in Fig. 10. Subsonic plasma flow at 300 A (Mach ~ 0.8) converts to transonic flow at 400 A (Mach ~ 1) at the outlet. The onset of supersonic flow structure formation is visible at 500 A

(Mach ~ 1.15) and the fully developed supersonic flow with shock diamonds is formed for 600 A (Mach ~ 1.4).

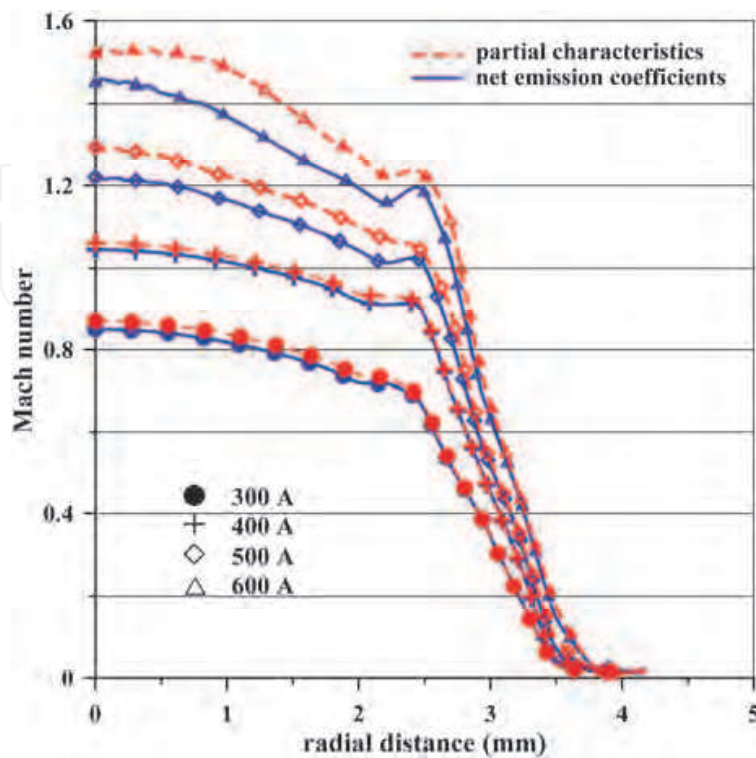


Fig. 9. Radial profiles of the Mach number 2 mm downstream of the nozzle exit, argon mass flow rate is 40 slm. The Mach numbers in the axial region are higher than 1 for currents equal to or higher than 400 A. Somewhat higher values of the Mach number provides the partial characteristics model.

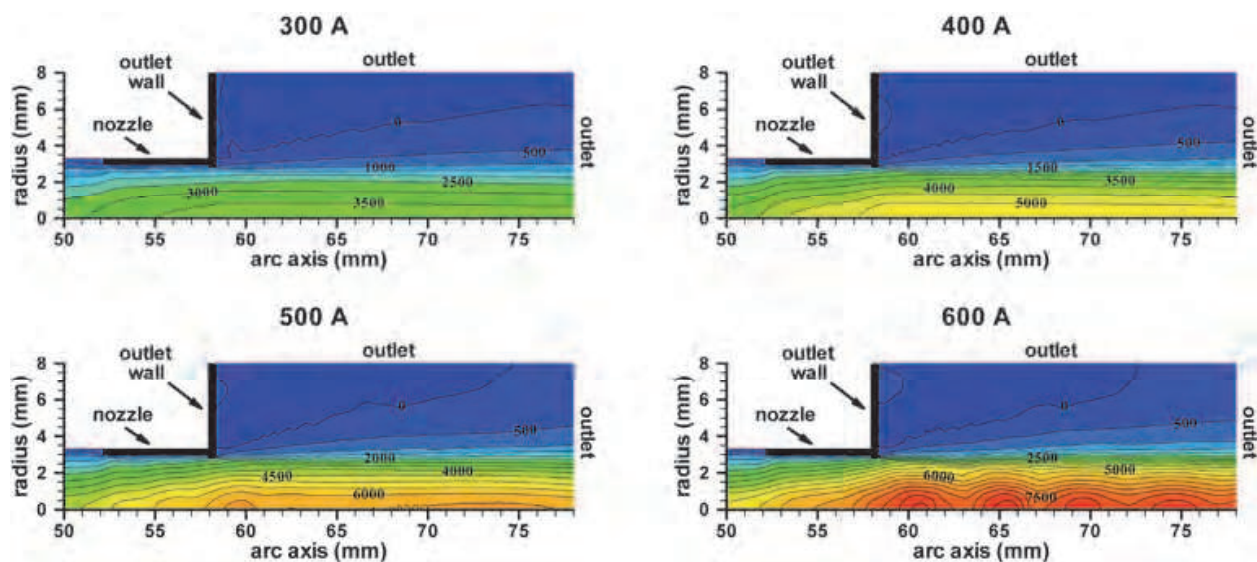


Fig. 10. Velocity contours in the outlet nozzle and near-discharge regions for 32 slm of argon. Partial characteristics radiation model is employed. Water mass flow rates are $0.228 \text{ g} \cdot \text{s}^{-1}$ (300 A), $0.315 \text{ g} \cdot \text{s}^{-1}$ (400 A), $0.329 \text{ g} \cdot \text{s}^{-1}$ (500 A), $0.363 \text{ g} \cdot \text{s}^{-1}$ (600 A), contour increments are $500 \text{ m} \cdot \text{s}^{-1}$. Supersonic flow structure is obvious for 600 A.

Values of temperature, voltage drop, the Mach number and overpressure as functions of arc current (300-600 A) and argon mass flow rate (22.5-40 slm) for the partial characteristics model are displayed in Fig. 11. Temperature and the Mach number shown here are taken at the arc axis 2 mm downstream of the outlet nozzle, the voltage drop and overpressure refer to the length of the discharge region of the hybrid-stabilized electric arc (58.32 mm). The maximum

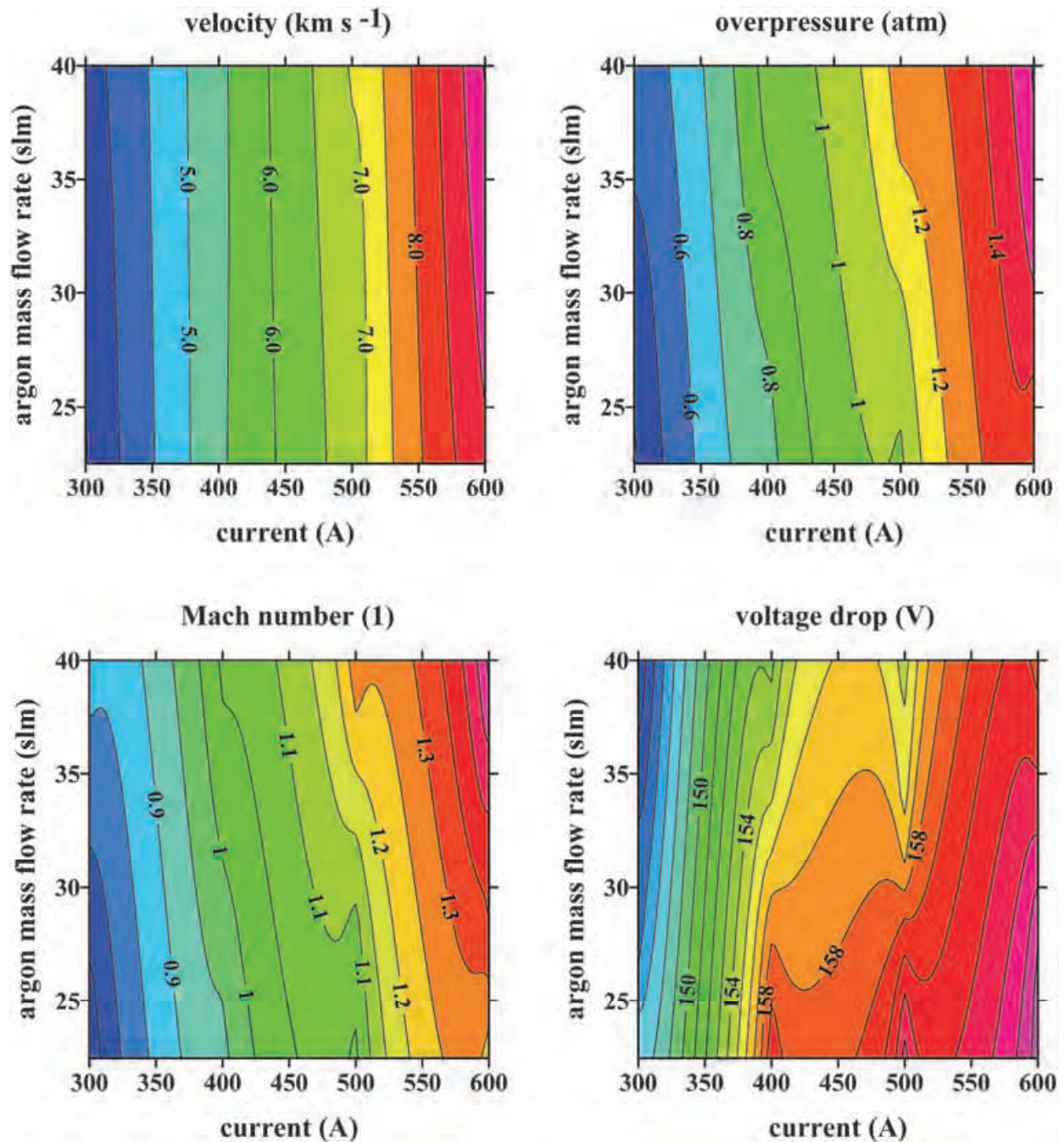


Fig. 11. Velocity (km s⁻¹), overpressure (atm), the Mach number and voltage drop (V) as functions of arc current (300-600 A) and argon mass flow rate (22.5-40 slm). Temperature and the Mach number are taken at the arc axis 2 mm downstream of the outlet nozzle, voltage drop and overpressure refer to the length of the discharge region of the hybrid-stabilized electric arc. Partial characteristics radiation model is employed.

values of the velocity ($9\,500\text{ m s}^{-1}$), overpressure (1.6 atm) and the Mach number (1.5) occur for 600 A and 40 slm of argon. It is evident from the slope of contours that overpressure and the Mach number increases with argon mass flow rate while the velocity increases only slightly. The transition from subsonic to supersonic flow occurs for currents around 400 A. The electric potential drop in the discharge chamber decreases with increasing argon mass flow rate, the maximum value reaches 164 V.

Temperature contours for the net emission and partial characteristics models are shown in Fig. 12. Temperature depicted is taken again at the arc axis 2 mm downstream of the outlet nozzle. Reabsorption of radiation increases temperature in arc fringes and decreases it near the arc axis, in the result the net emission model provides higher axial temperatures.

The slight increase of velocity with argon mass flow rate has thus an apparent explanation: on one hand, the increase of argon mass flow rate implies the corresponding increase of velocity. On the other hand, temperature decreases with argon mass flow rate, lowering thus the increase of plasma velocity.

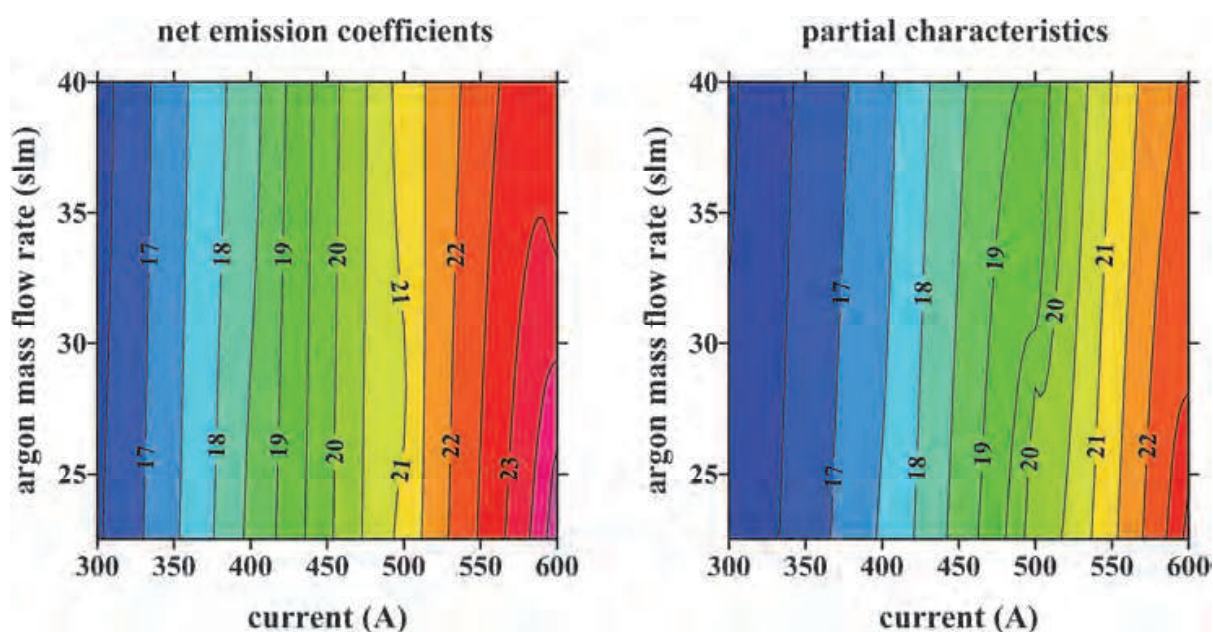


Fig. 12. Temperature contours (kK) in dependence of arc current (300-600 A) and argon mass flow rate (22.5-40 slm) for the net emission and partial characteristics models. Temperature depicted is taken at the arc axis 2 mm downstream of the outlet nozzle. Reabsorption of radiation slightly decreases axial temperatures.

3.2 Comparison of radial temperature and velocity profiles with experiments

A number of experiments have been carried out on the hybrid-stabilized electric arc in recent past for the currents 300-600 A with 22-40 slm of argon. Temperature is one of the fundamental plasma parameters, needed also for evaluation of the other quantities.

In experiment, the radial profiles of temperature at the nozzle exit were calculated from optical emission spectroscopy measurements. The procedure is based on the ratio of emission coefficients of hydrogen H_{β} line and four argon ionic lines using calculated LTE composition of the plasma for various argon mole fractions as a function of temperature (Křenek, 2008). From the calculated molar fractions of hydrogen and argon it is easy to obtain emission coefficients of H_{β} and argon lines. The temperature corresponding to an

experimental ratio of emission coefficients is then found by cubic spline interpolation on the theoretical data.

Fig. 13 compares measured and calculated temperature profiles 2 mm downstream of the nozzle exit for 300-600 A and 22.5 slm of argon. Excellent agreement is demonstrated for 300 and 600 A where the measured profiles nearly coincide with the two profiles calculated using the net emission and partial characteristics radiation methods. For 400 and 500 A agreement is better for the profiles calculated by the net emission coefficients (black color).

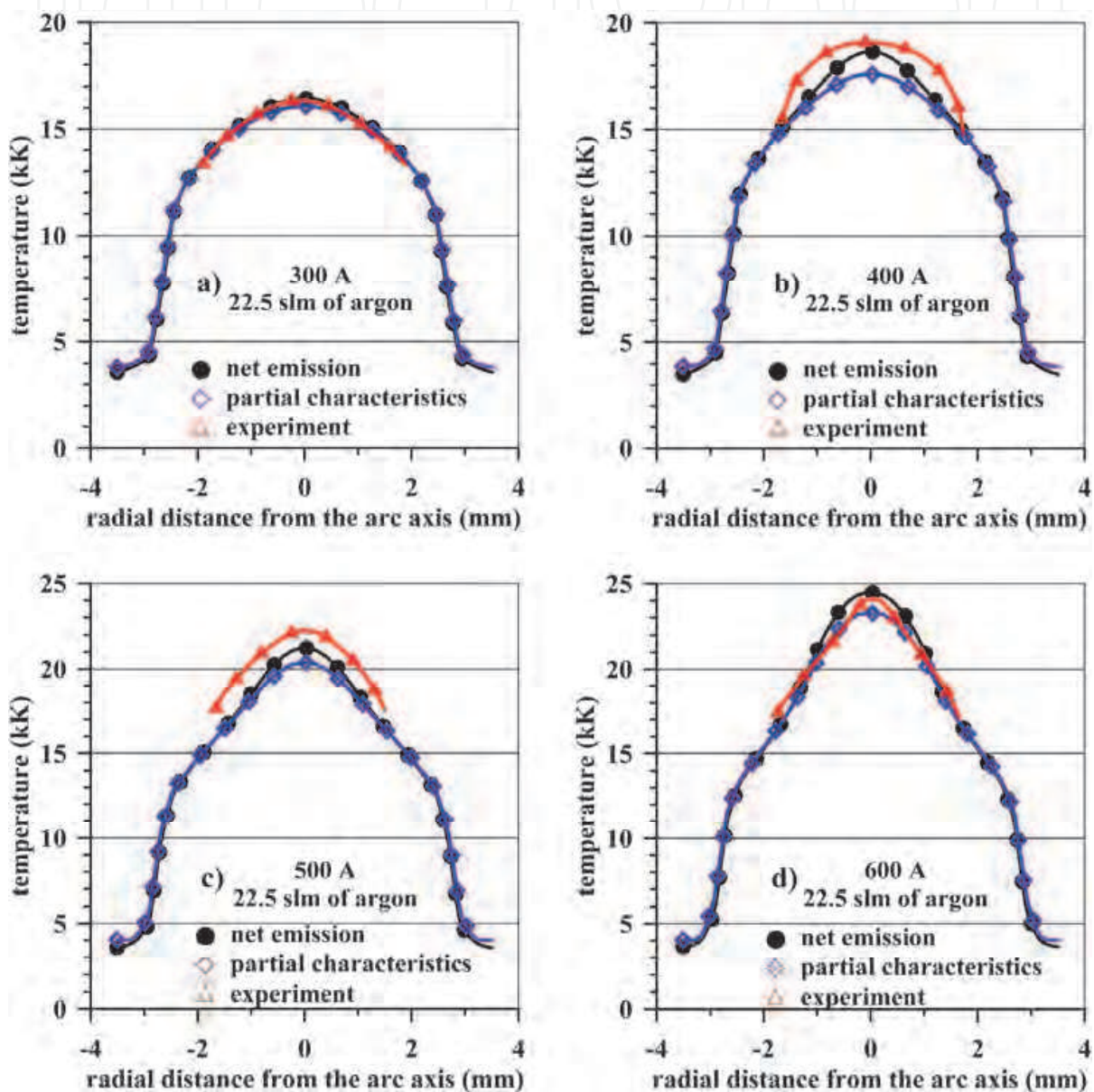


Fig. 13. Experimental and calculated radial temperature profiles 2 mm downstream of the nozzle exit for 300-600 A and 22.5 slm of argon.

Relative difference between the calculated and experimental values of temperature at the arc axis 2 mm downstream of the nozzle exit has been evaluated for broad range of currents and argon mass flow rates. The relative difference is defined here as

$$\Delta = 100 \cdot \text{abs}(T_{num} - T_{exp}) / T_{num} ,$$

where T_{num} (T_{exp}) are the values of the calculated (experimental) temperature. It was proved that the maximum relative difference between the calculated and experimental temperature profiles is lower than 10% for the partial characteristics and 5% for the net emission radiation model used in the present calculation, i.e. the net emission radiation model gives better agreement with experiment as regards axial temperatures.

Comparison of the measured and calculated temperature profiles with our former calculations (Jeništa et al., 2010) is shown in Fig. 14 for 500 and 600 A. The set of profiles is calculated/measured again 2 mm downstream of the nozzle exit. The term "new model" introduced here refers to the present model with the assumptions described in Secs. 2.1, 2.2, while the "old model" means the former one with the following assumptions:

- a. the transport and thermodynamic properties of the argon-water plasma mixture are calculated using linear mixing rules for non-reacting gases based either on mole or mass fractions of argon and water species (Jeništa et al., 2010),
- b. all the transport and thermodynamic properties as well as the radiation losses are dependent on temperature, and argon molar content but NOT dependent on pressure,
- c. radiation transitions of H_2O molecule are omitted.

In our present model 1) all the transport and thermodynamic properties are calculated according to the Chapman-Enskog method in the 4th approximation; 2) all the properties are dependent on pressure; 3) radiation transitions of H_2O molecule are considered. It is obvious that radial temperature profiles obtained by our "old model" give worse comparison with experiments - higher temperatures and flatter profiles compared to our present calculation. Similar results were obtained also for the net emission model. Improvements in the properties caused better convergence between the experiment and calculation.

More comprehensive view on the closeness of the calculated and experimental temperature profiles offers Fig. 15. The dots in the plot represent the so-called "average relative difference of temperature" defined as

$$\Delta_{av}^T = \frac{100}{N} \cdot \sum_{i=1}^N \text{abs}(T_{num}^i - T_{exp}^i) / T_{num}^i ,$$

estimating a sort of average relative difference along the temperature profile, N is the number of available coincident numerical T_{num}^i and experimental T_{exp}^i values of temperature along the radius. It is apparent that our present "new model" gives better comparison than the "old model" in all cases.

Besides temperature profiles, velocity profiles at the nozzle exit and mass and momentum fluxes through the torch nozzle are important indicators for characterization of the plasma torch performance. In experiment, velocity at the nozzle exit is being determined from the measured temperature profile and power balance assuming local thermodynamic equilibrium (Kavka et al., 2008). First, the Mach number M is obtained from the simplified energy equation integrated through the discharge volume (Jeništa, 1999b); second, the velocity profile is derived from the measured temperature profile using the definition of the Mach number

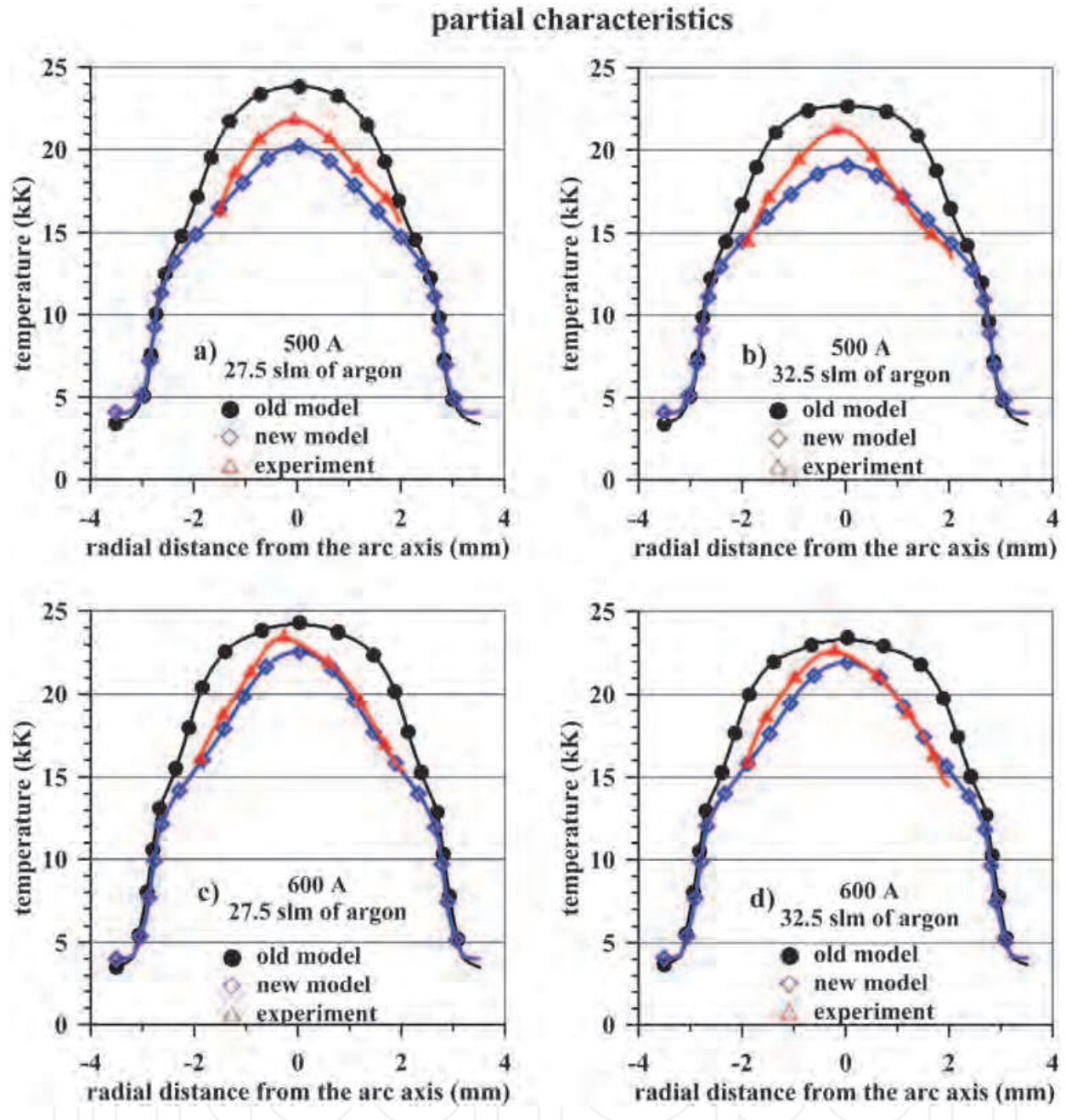


Fig. 14. Experimental and calculated radial temperature profiles 2 mm downstream of the nozzle exit for 500 and 600 A with 27 and 32 slm of argon, partial characteristics method. The so-called „new model“ stands for the present model, the „old model“ presents our previous model with simplified plasma properties (see the text).

$$u(r) = M \cdot c\{T(r)\},$$

where $c\{T(r)\}$ is the sonic velocity for the experimental temperature profile estimated from the T&TWinner code (Pateyron, 2009). The drawback of this method is the assumption of the constant Mach number over the nozzle radius. Nevertheless the existence of supersonic

regime (i.e., the mean value of the Mach number over the nozzle exit higher than 1) using this method was proved for 500 A and 40 slm of argon, as well as for 600 A for argon mass flow rates higher than 27.5 slm. Similar results have been also reported in our previous work (Jeništa et al., 2008).

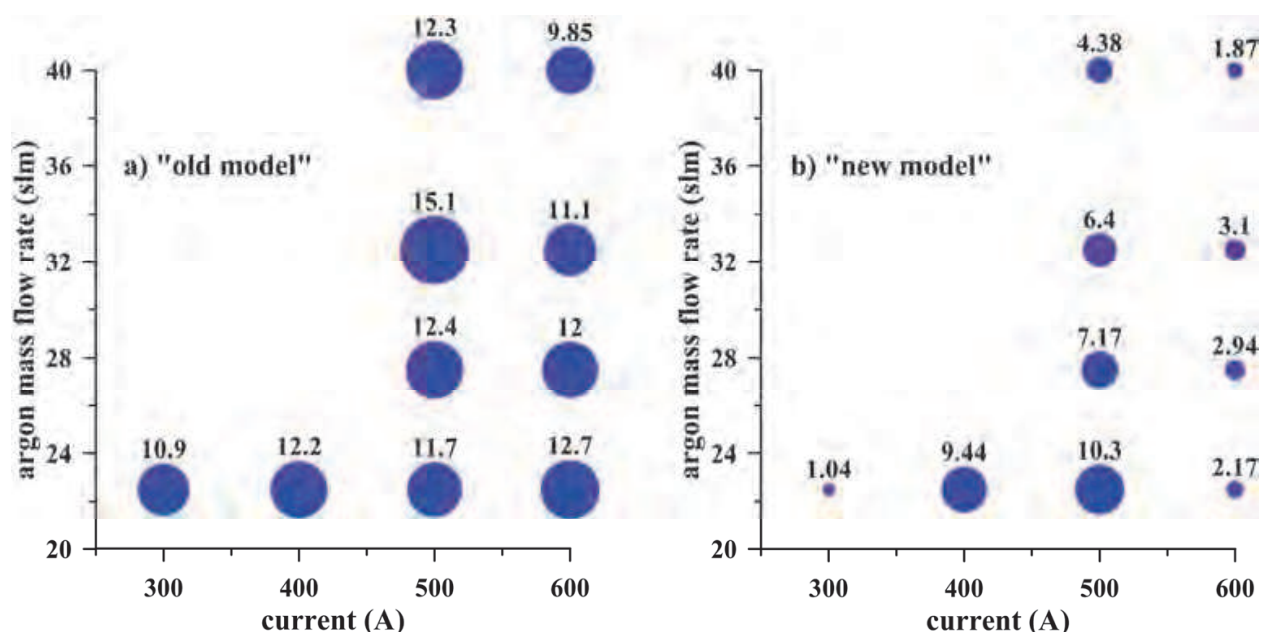


Fig. 15. Average relative difference (see the text) between the calculated and experimental radial temperature profiles, shown in %, at the axial position 2 mm downstream of the nozzle exit, partial characteristics. The so-called „new model” stands for the present model, exhibiting better agreement with experiments; the „old model” presents our previous model with simplified plasma properties (see the text).

For more exact evaluation of velocity profiles we employed the so-called “integrated approach”, i.e., exploitation of both experimental and numerical results: velocity profiles are determined as a product of the Mach number profiles obtained from the present numerical simulation and the sonic velocity based on the experimental temperature profiles. The results for 300-600 A with 22.5 slm of argon for the partial characteristics method are displayed in Fig. 16. Each graph contains four curves - velocity profiles based on the “new” and “old” models (see above), the experimental velocity profile and the velocity profile obtained by the “integrated approach” (the blue curves), we will call it “re-calculated” velocity profile. It is clearly visible that agreement of such re-calculated experimental velocity profiles with the numerical ones is much better than between original experiments and calculation. High discrepancy between the “old” and “new” velocity profiles is also apparent, especially for lower currents.

Fig. 17 presents the same type of plot as is presented in Fig. 15 but with the analogous definition of the “average relative difference of velocity”

$$\Delta_{av}^u = \frac{100}{M} \cdot \sum_{i=1}^M \text{abs}(u_{re-exp}^i - u_{exp}^i) / u_{re-exp}^i ,$$

where u_{re-exp}^i is the re-calculated velocity and u_{exp}^i is the experimental velocity at the point i , M is the number of available points at which the difference is being evaluated. It is again evident that the present “new model” gives in most cases much lower relative difference than the “old model” for all studied cases.

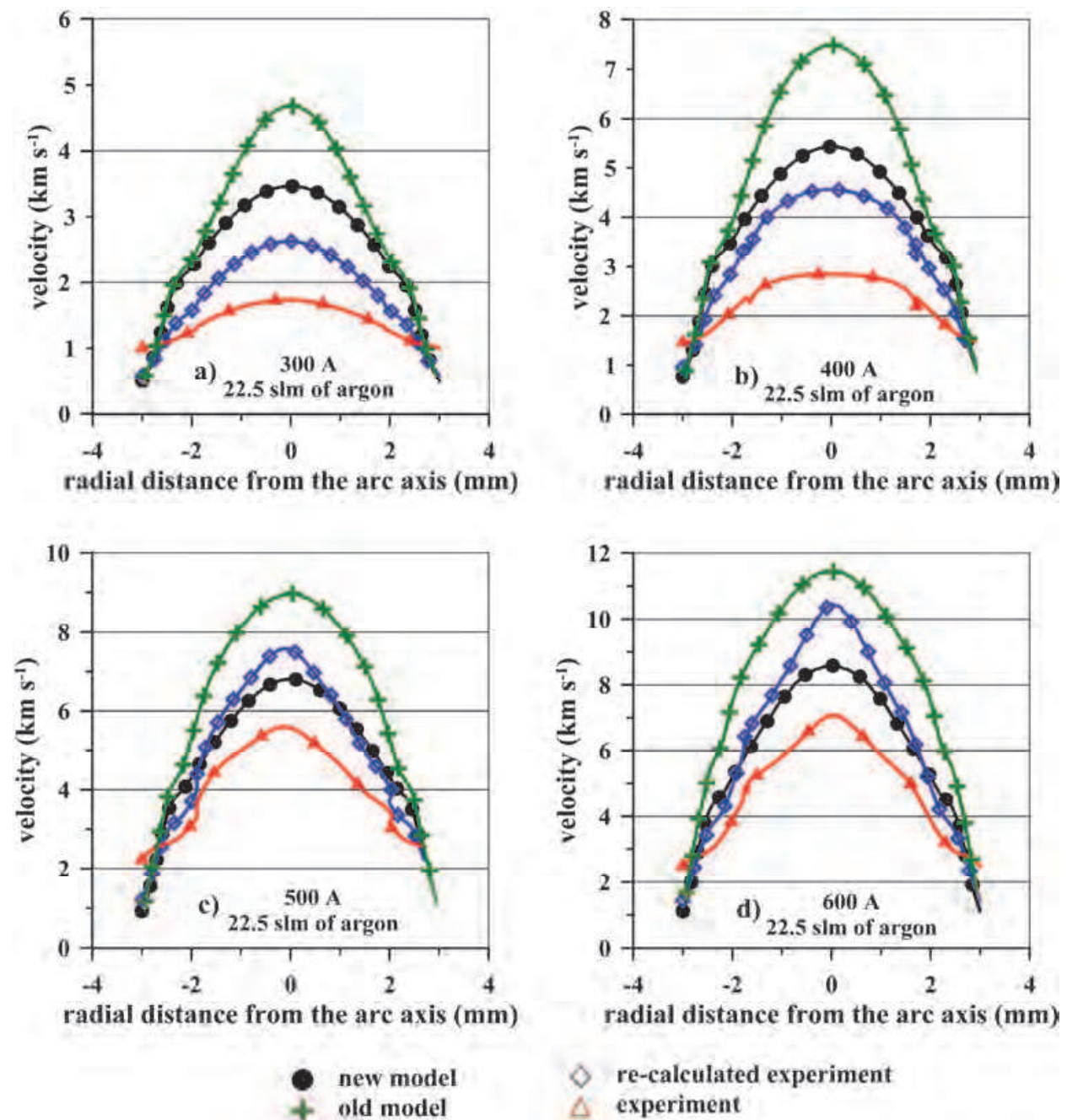


Fig. 16. Velocity profiles 2 mm downstream of the nozzle exit for 300 - 600 A with 22.5 slm of argon. Calculation – partial characteristics model, re-calculated experimental profile is based on the experimental temperature profile and calculated Mach number (see the text). The so-called „new model” stands for the present model, the „old model” presents our previous model with simplified plasma properties (see the text). The re-calculated velocity profiles show better agreement with the experiment.

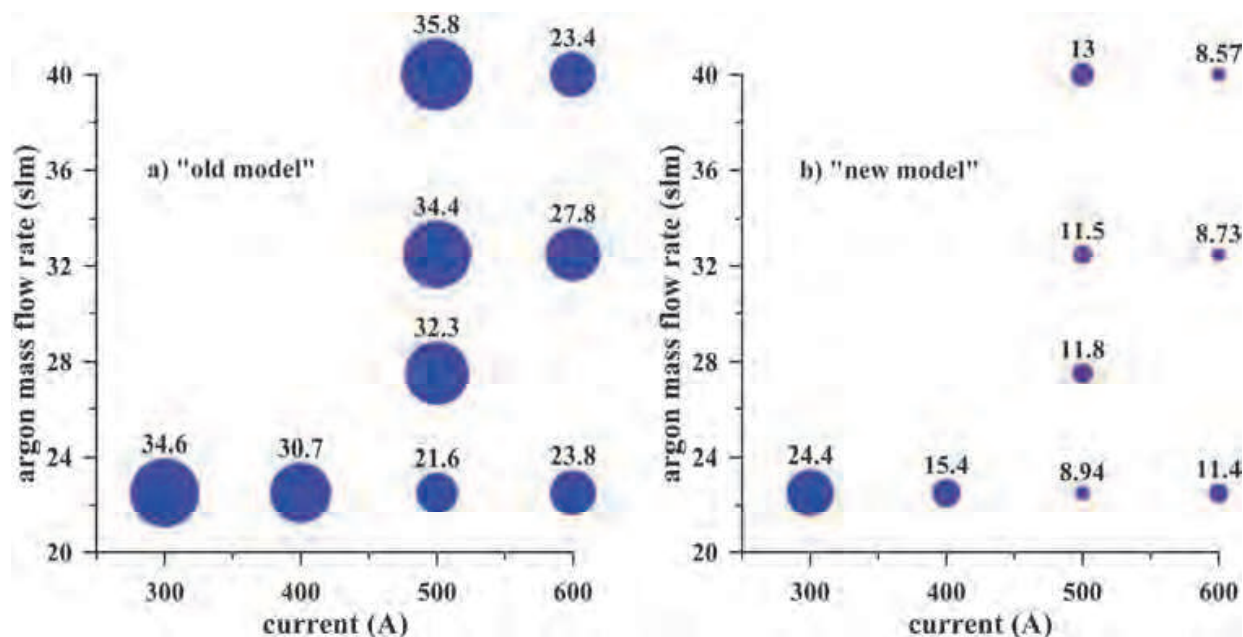


Fig. 17. Average relative difference (see the text) between the calculated and re-calculated (the experimental temperature profile and the calculated Mach number) radial velocity profiles, shown in % at the axial position 2 mm downstream of the nozzle exit, partial characteristics. The so-called „new model“ stands again for the present model and exhibits better agreement with experiments than the „old model“.

3.3 Power losses from the arc

Energy balance, responsible for performance of the hybrid-stabilized argon-water electric arc, is illustrated in the last set of figures. Fig. 18 (left) demonstrates the arc efficiency and the power losses from the arc discharge as a function of current for 40 slm of argon. The arc efficiency is defined here as $\eta = 1 - (\text{power losses}) / (\Delta U \cdot I)$ with ΔU being the electric potential drop in the discharge chamber and I the current. The power losses from the arc stand for the conduction power lost from the arc in the radial direction and the radiation power leaving the discharge, which are considered to be the two principal processes responsible for the power losses. The ratio of the power losses to the input power in the discharge chamber $\Delta U \cdot I$ is indicated as the power losses in a per cent scale: the maximum difference of about 2-4 % between the net emission and partial characteristics methods is obviously caused by the amount of radiation reabsorbed in colder arc regions, the partial characteristics provides lower power losses. The arc efficiency is relatively high and ranges between 77-82 % for the net emission model and 80-84 % for the partial characteristics. The power losses slightly increases with increasing argon mass flow rate and with decreasing current, see Fig. 18 (right).

Fig. 19 (left) displays the typical radial profiles of temperature, divergence of radiation flux and radiation flux for 600 A and argon mass flow rate of 40 slm. Axial position is 4 cm from the argon inlet nozzle, i.e., inside the discharge chamber. Temperature reaches 24 700 K at the axis and declines to 773 K at the edge of the calculation domain. The radiation flux reaches $9.7 \cdot 10^6 \text{ W} \cdot \text{m}^{-2}$ at the arc edge with the maximum magnitude $3.1 \cdot 10^7 \text{ W} \cdot \text{m}^{-2}$ at the radial distance of 2.2 mm. The divergence of radiation flux becomes negative at the radial distance

over 2.6 mm, i.e., the radiation is being reabsorbed in this region. Despite the negative values of the divergence of radiation flux in arc fringes are relatively small compared to the positive ones in the axial region, the amount of reabsorbed radiation is 32.4% (understand: ratio of the negative and positive contributions of the divergence of radiation flux, see below) because the plasma volume increases with the third power of radius.

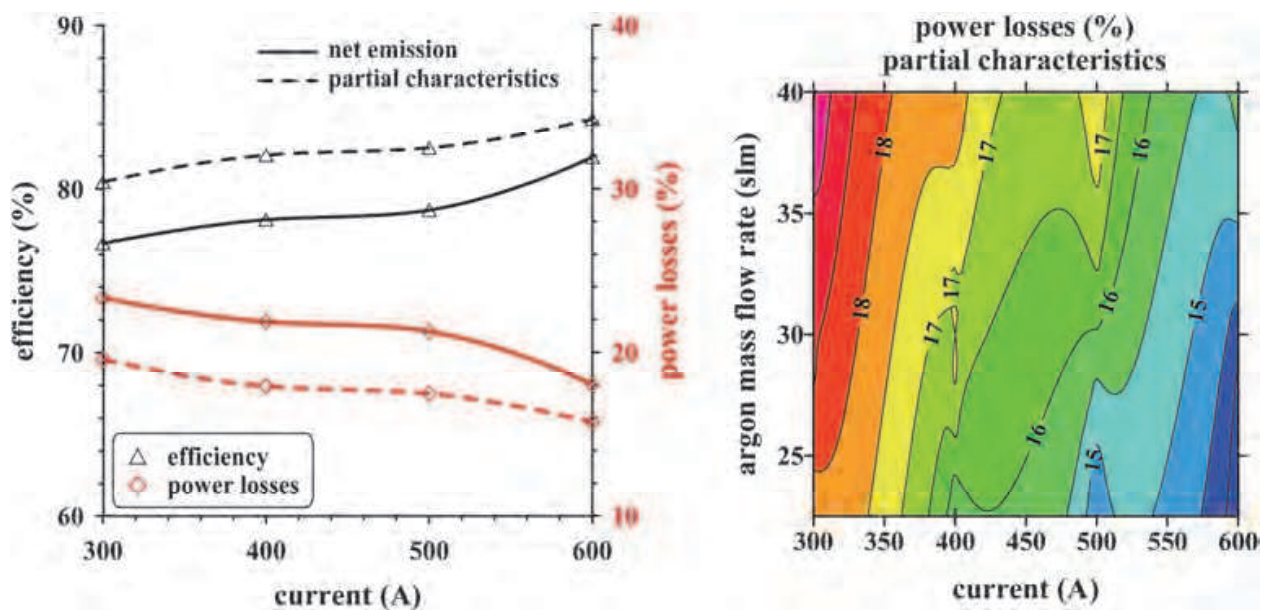


Fig. 18. Power losses and arc efficiency as functions of arc current for 40 slm of argon (left). The arc efficiency (%) is defined as $\eta = 1 - (\text{power losses}) / (\Delta U \cdot I)$, where the power losses are due to radiation and radial conduction. Power losses in % is the ratio $\text{power losses} / (\Delta U \cdot I)$, shown also in dependence of current and argon mass flow rate (right).

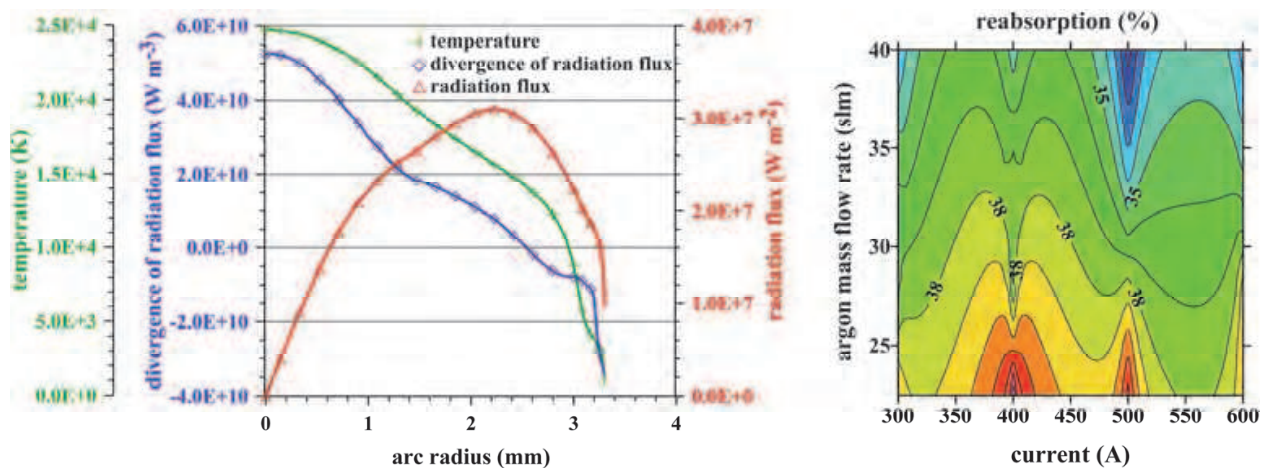


Fig. 19. Radial profiles of temperature, divergence of radiation flux and radiation flux for 600 A and argon mass flow rate of 40 slm inside the discharge chamber at the axial position of 4 cm (left); partial characteristics. Reabsorption of radiation occurs at ~ 2.6 mm from the axis. Reabsorption of radiation (right) for different currents and argon mass flow rates is defined as the ratio of the negative to the positive contributions of the divergence of radiation flux - it ranges between 30-45 % and slightly decreases for higher argon mass flow rates.

Fig. 19 (right) shows the amount of reabsorbed radiation (%) in argon-water mixture plasma within the arc discharge for the currents 300-600 A as a function of argon mass flow rate. The negative and positive parts of the divergence of radiation flux are integrated through the discharge volume. Reabsorption defined here is the ratio of the negative and positive contributions of the divergence of radiation flux - it ranges between 31-45 % and increases for lower contents of argon in the mixture.

Direct comparison of the amount of reabsorbed radiation with experiments is unavailable, however the indirect sign of validity of our results is a very good agreement between the experimental and calculated radial temperature profiles two millimeters downstream of the outlet nozzle presented above.

4. Conclusions

The numerical model for an electric arc in the plasma torch with the so-called hybrid stabilization, i.e., combined stabilization of arc by gas and water vortex, has been presented. To study possible compressible phenomena in the plasma jet, calculations have been carried out for the interval of currents 300-600 A and for relatively high argon mass flow rates between 22.5 slm and 40 slm. The partial characteristics as well as the net emission coefficients methods for radiation losses from the arc are employed. The results of the present calculation can be summarized as follows:

- a. The numerical results proved that transition to supersonic regime starts around 400 A. The supersonic structure with shock diamonds occurs in the central parts of the discharge at the outlet region. The computed profiles of axial velocity, pressure and temperature correspond to an under-expanded atmospheric-pressure plasma jet.
- b. The partial characteristics radiation model gives slightly lower temperatures but higher outlet velocities and the Mach numbers compared to the net emission model.
- c. Reabsorption of radiation ranges between 31-45 %, it decreases with current and also slightly decreases with argon mass flow rate. The arc efficiency reaches up to 77-84%, the power losses from the arc due to radiation and radial conduction are between 16-24%.
- d. It was proved that simulations for laminar and turbulent regimes give nearly the same results, so that the plasma flow can be considered to be laminar for the operating conditions and a simplified discharge geometry studied in this paper.
- e. Comparison with available experimental data proved very good agreement for temperature - the maximum relative difference between the calculated and experimental temperature profiles is lower than 10% for the partial characteristics and 5% for the net emission radiation model used in the present calculation. Calculated radial velocity profiles 2 mm downstream of the nozzle exit show good agreement with the ones evaluated from the combination of calculation and experiment (integrated approach). Agreement between the calculated radial velocity profiles and the profiles analyzed purely from experimental data is worse. Evaluation of the Mach number from the experimental data for 500 and 600 A give values higher than one close to the exit nozzle, it thus proves the existence of the supersonic flow regime. The present numerical model provides also better agreement with experiments than our previous model based on the simplified transport, thermodynamic and radiation properties of argon-water plasma mixture.

The existing numerical model will be further extended to study the effect of mixing of plasma species within the hybrid arc discharge by the binary diffusion coefficients (Murphy, 1993, 2001) for three species - hydrogen, argon and oxygen.

5. Acknowledgments

J. Jeništa is grateful for financial support under the Fluid Science International COE Program from the Institute of Fluid Science, Tohoku University, Sendai, Japan, and their computer facilities. Financial support from the projects GA CR 205/11/2070 and M100430901 from the Academy of Sciences AS CR, v.v.i., is gratefully acknowledged. Our appreciation goes also to the Institute of Physics AS CR, v.v.i., for granting their computational resources (Luna/Apollo grids). The access to the METACentrum supercomputing facilities provided under the research intent MSM6383917201 is highly appreciated.

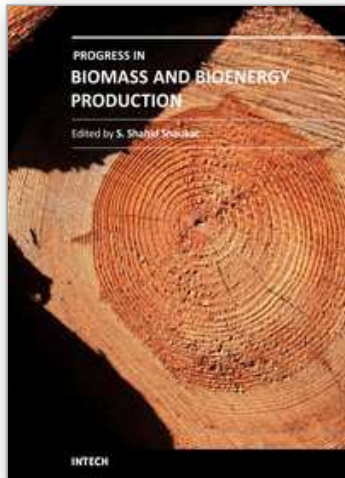
6. References

- Bartlová, M. & Aubrecht, V. (2006). Photoabsorption of diatomic molecules. *Czechoslovak Journal of Physics*, Vol. 56, Suppl. B, (June 2006), pp. B632-B637, ISSN 0011-4626.
- Březina, V.; Hrabovský, M.; Konrád M.; Kopecký, V. & Sember, V. (2001). New plasma spraying torch with combined gas-liquid stabilization of arc, *Proceedings of 15th International Symposium on Plasma Chemistry (ISPC 15)*, pp. 1021-1026, ISBN non-applicable, Orleans, France, July 9-13, 2001.
- Hrabovský, M.; Konrád M.; Kopecký, V. & Sember, V. (1997). Processes and properties of electric arc stabilized by water vortex. *IEEE Transactions on Plasma Science*, Vol. 25, No.5, (October 1997), pp. 833-839, ISSN 0093-3813.
- Hrabovský, M.; Kopecký, V. & Sember, V. (2003). Effect of Gas Properties on Characteristics of Hybrid Gas/Water Plasma Spraying Torch, *Proceedings of 16-th International Symposium on Plasma Chemistry (ISPC 16)*, on CD-ROM, ISBN non-applicable, Taormina, Italy, June 22-27, 2003.
- Hrabovský, M.; Kopecký, V.; Sember, V.; Kavka, T.; Chumak, O. & Konrád, M. (2006). Properties of hybrid water/gas DC arc plasma torch, *IEEE Transactions on Plasma Science*, Vol. 34, No.4, (August 2006), pp. 1566-1575, ISSN 0093-3813.
- Jameson, A. & Yoon, S. (1987). Lower-upper implicit schemes with multiple grids for the Euler equations. *AIAA Journal*, Vol. 25, No. 7, (July 1987), pp. 929-935, ISSN 0001-1452, E-ISSN 1533-385X.
- Jeništa, J.; Kopecký, V. & Hrabovský, M. (1999a). Effect of vortex motion of stabilizing liquid wall on properties of arc in water plasma torch, In: *Heat and mass transfer under plasma conditions*, editors: Fauchais, P.; Mullen, van der J. & Heberlein, J., pp. 64-71, Annals of the New York Academy of Sciences, Vol. 891, ISBN 1-57331-234-7 (cloth), ISBN 1-57331-235-5 (paper), ISSN 0077-8923, New York.
- Jeništa, J. (1999b). Water-vortex stabilized electric arc: I. Numerical model. *Journal of Physics D: Applied Physics*, Vol. 32, No. 21, (November 1999), pp. 2763-2776, ISSN 0022-3727 (print), ISSN 1361-6463 (online).
- Jeništa, J. (2003a). Water-vortex stabilized electric arc: III. Radial energy transport, determination of water-vapour-boundary and arc performance. *Journal of Physics D: Applied Physics*, Vol. 36, No. 23, (December 2003), pp. 2995-3006, ISSN 0022-3727 (print), ISSN 1361-6463 (online).
- Jeništa, J. (2003b). The effect of different regimes of operation on parameters of a water-vortex stabilized electric arc. *Journal of High Temperature Material Processes*, Vol. 7, No. 1, (March 2003), pp. 11-16, ISSN 1093-3611 (print), ISSN 1940-4360 (online).

- Jeništa, J. (2004). Numerical modeling of hybrid stabilized electric arc with uniform mixing of gases. *IEEE Transactions on Plasma Science*, Vol. 32, No. 2, (April 2004), pp. 464-472, ISSN 0093-3813.
- Jeništa, J.; Bartlová, M. & Aubrecht, V. (2007). The impact of molecular radiation processes in water plasma on performance of water-vortex and hybrid-stabilized electric arcs, *PPPS-2007 Proceedings of the 34th IEEE International Conference on Plasma Science and The 16th IEEE International Pulsed Power Conference*, pp. 1429-1432, ISBN 1-4244-0914-4, Albuquerque, New Mexico, USA, June 17-22, 2007.
- Jeništa, J.; Takana, H.; Hrabovský, M. & Nishiyama, H. (2008). Numerical investigation of supersonic hybrid argon-water-stabilized arc for biomass gasification. *IEEE Transactions on Plasma Science*, Vol. 36, No. 4, (August 2008), pp.1060-1061, ISSN 0093-3813.
- Jeništa, J.; Takana, H.; Nishiyama, H.; Bartlova, M.; Aubrecht, V. & Hrabovský, M. (2010). Parametric study of hybrid argon-water stabilized arc under subsonic and supersonic regimes. *Journal of High Temperature Material Processes*, Vol. 14, No. 1-2, (April 2010), pp. 63-76, ISSN 1093-3611 (print), ISSN 1940-4360 (online).
- Kavka, T.; Chumak, O.; Sember, V. & Hrabovský, M. (2007). Processes in Gerdien arc generated by hybrid gas-water torch, *Proceedings of XXVIII International Conference on Phenomena in Ionized Gases (ICPIG 2007)*, pp. 1819-1822, ISBN 978-80-87026-01-4, Prague, Czech Republic, July 15-20, 2007.
- Kavka, T.; Maslani, A.; Chumak, O. & Hrabovský, M. (2008). Character of plasma flow at the exit of DC arc gas-water torch, *Proceedings of 5-th International Conference on Flow Dynamics*, pp. OS8-11, ISBN non-applicable, Sendai, Japan, November 17-19, 2008.
- Křenek, P. & Něnička, V. (1984). Calculation of transport coefficients of a gas mixture in the 4-th approximation of Enskog-Chapman theory. *Acta Technica CSAV*, Vol. 28, No. 4, (1984), pp. 420-433, ISSN 0001-7043.
- Křenek, P. (2008). Thermophysical properties of H₂O–Ar plasmas at temperatures 400–50,000 K and pressure 0.1 MPa. *Plasma Chemistry and Plasma Processes*, Vol. 28, No. 1, (January 2008), pp. 107-122, ISSN 0272-4324.
- Leer, van B. (1979). Towards the ultimate conservative difference scheme. V. A second-order sequel to Godunov's method. *Journal of Computational Physics*, Vol. 32, No. 1, (July 1979), pp. 101-136, ISSN 0021-9991.
- Murphy, A. B. (1993). Diffusion in equilibrium mixtures of ionized gases, *Physical Review E*, Vol. 48, No. 5, (November 1993), pp. 3594-3603, ISSN 1539-3755 (print), ISSN 1550-2376 (online).
- Murphy, A. B. (2001). Thermal plasmas in gas mixtures, *Journal of Physics D: Applied Physics*, Vol. 34, No. 20-21, (October 2001), pp. R151–R173, ISSN 0022-3727 (print), ISSN 1361-6463 (online).
- Patankar, S. V. (1980). *Numerical Heat Transfer and Fluid Flow*, McGraw-Hill, ISBN 0-07-048740-5, New York.
- Pateyron, B. & Katsonis, C. (2009). T&TWinner, available from: <http://ttwinner.free.fr/>.
- Roe, P. L. (1981). Approximate Riemann solvers, parameter vectors, and difference schemes. *Journal of Computational Physics*, Vol. 43, No. 2, (October 1981), pp. 357-372, ISSN 0021-9991.
- Van Oost, G.; Hrabovský, M.; Kopecký, V.; Konrád, M.; Hlína, M.; Kavka, T.; Chumak, O.; Beeckman, E. & Verstraeten, J. (2006). Pyrolysis of waste using a hybrid argon-

- water stabilized torch, *Vacuum*, Vol. 80, No. 11-12, (September 2006), pp. 1132-1137, ISSN 0042-207X.
- Van Oost, G.; Hrabovský, M.; Kopecký, V.; Konrád, M.; Hlína, M.; Kavka, T. (2008). Pyrolysis/gasification of biomass for synthetic fuel production using a hybrid gas-water stabilized plasma torch. *Vacuum*, Vol. 83, No. 1, (September 2008), pp. 209-212, ISSN 0042-207X.
- Yoon, S. & Jameson, A. (1988). Lower-upper symmetric-Gauss-Seidel method for the Euler and Navier-Stokes equations. *AIAA Journal*, Vol. 26, No. 9, (September 1988), pp. 1025-1026, ISSN 0001-1452, E-ISSN 1533-385X.

IntechOpen



Progress in Biomass and Bioenergy Production

Edited by Dr. Shahid Shaukat

ISBN 978-953-307-491-7

Hard cover, 444 pages

Publisher InTech

Published online 27, July, 2011

Published in print edition July, 2011

Alternative energy sources have become a hot topic in recent years. The supply of fossil fuel, which provides about 95 percent of total energy demand today, will eventually run out in a few decades. By contrast, biomass and biofuel have the potential to become one of the major global primary energy source along with other alternate energy sources in the years to come. A wide variety of biomass conversion options with different performance characteristics exists. The goal of this book is to provide the readers with current state of art about biomass and bioenergy production and some other environmental technologies such as Wastewater treatment, Biosorption and Bio-economics. Organized around providing recent methodology, current state of modelling and techniques of parameter estimation in gasification process are presented at length. As such, this volume can be used by undergraduate and graduate students as a reference book and by the researchers and environmental engineers for reviewing the current state of knowledge on biomass and bioenergy production, biosorption and wastewater treatment.

How to reference

In order to correctly reference this scholarly work, feel free to copy and paste the following:

Jiří Jeništa, Hidemasa Takana, Hideya Nishiyama, Milada Bartlová, Vladimír Aubrecht, Petr Křenek, Milan Hrabovsky, Tetyana Kavka, Viktor Sember and Alan Mašláni (2011). Numerical Investigation of Hybrid-Stabilized Argon-Water Electric Arc Used for Biomass Gasification, Progress in Biomass and Bioenergy Production, Dr. Shahid Shaukat (Ed.), ISBN: 978-953-307-491-7, InTech, Available from: <http://www.intechopen.com/books/progress-in-biomass-and-bioenergy-production/numerical-investigation-of-hybrid-stabilized-argon-water-electric-arc-used-for-biomass-gasification>

INTECH
open science | open minds

InTech Europe

University Campus STeP Ri
Slavka Krautzeka 83/A
51000 Rijeka, Croatia
Phone: +385 (51) 770 447
Fax: +385 (51) 686 166
www.intechopen.com

InTech China

Unit 405, Office Block, Hotel Equatorial Shanghai
No.65, Yan An Road (West), Shanghai, 200040, China
中国上海市延安西路65号上海国际贵都大饭店办公楼405单元
Phone: +86-21-62489820
Fax: +86-21-62489821

© 2011 The Author(s). Licensee IntechOpen. This chapter is distributed under the terms of the [Creative Commons Attribution-NonCommercial-ShareAlike-3.0 License](#), which permits use, distribution and reproduction for non-commercial purposes, provided the original is properly cited and derivative works building on this content are distributed under the same license.

IntechOpen

IntechOpen